BRNO UNIVERSITY OF TECHNOLOGY
VYSOKÉ UČENÍ TECHNICKÉ V BRNĚ

FACULTY OF MECHANICAL ENGINEERING
FAKULTA STROJNÍHO INŽENÝRSTVÍ

INSTITUTE OF AEROSPACE ENGINEERING
LETECKÝ ÚSTAV

THERMAL CONTACT RESISTANCE OF PLANAR SURFACES
TEPELNÝ PŘECHODOVÝ ODPOR PLOŠNÝCH KONTAKTŮ

BACHELOR'S THESIS
BAKALÁŘSKÁ PRÁCE

AUTHOR — **Timko Marek Mateášik**
AUTOR PRÁCE

SUPERVISOR — **Ing. Jakub Mašek**
VEDOUCÍ PRÁCE

BRNO 2019

BRNO UNIVERSITY OF TECHNOLOGY
FACULTY OF MECHANICAL ENGINEERING

Bachelor's Thesis Assignment

Institut:	Institute of Aerospace Engineering
Student:	**Timko Marek Mateášik**
Degree programm:	Engineering
Branch:	Fundamentals of Mechanical Engineering
Supervisor:	**Ing. Jakub Mašek**
Academic year:	2018/19

As provided for by the Act No. 111/98 Coll. on higher education institutions and the BUT Study and Examination Regulations, the director of the Institute hereby assigns the following topic of Bachelor's Thesis:

Thermal contact resistance of planar surfaces

Brief description:

The development of the space Heat Switch involves solutions of the heat conduction through specific components and their contacts. The design of the Heat Switch defines several surface contacts of different materials and dimensions. The heat transfer - minimum effective thermal resistance – through the planar contact is an important key to achieve the maximum thermal conductivity of the switch.

Bachelor's Thesis goals:

- Description of parameters influencing the thermal resistance of the planar contacts and the possible solutions on the Switch
- Describe mathematical models of planar contacts thermal resistance
- Design and production of test specimens from materials used in the Switch design
- Results evaluation of measured thermal resistances
- Comparison of experimental thermal resistance data with the theoretical model

Recommended bibliography:

YOVANOVICH, M.M., J.R. CULHAM a P. TEERTSTRA. Calculating interface resistance. Electronics Cooling. 1997, 3(2), 24-29.

Students are required to submit the thesis within the deadlines stated in the schedule of the academic year 2018/19.

In Brno, 25. 10. 2018

L. S.

doc. Ing. Jaroslav Juračka, Ph.D.
Director of the Institute

doc. Ing. Jaroslav Katolický, Ph.D.
FME dean

Summary

Bachelor‘s thesis examines the thermal contact resistance of planar surfaces for purposes of miniaturised heat switch project. The thesis focuses on finding of suitable mathematical model for prediction of thermal contact resistance as one of the possible solutions for miniaturized heat switch optimization. This work consists of theoretical and practical part.

Theoretical part briefly introduce a background of the project and the reason for initiation of this work. This work, further examines the definition of thermal contact resistance and factors that influence it. Subsequently introduce a review of existing models for prediction of thermal contact resistance, appropriate selection of models for the possible use and their description.

Practical part examines the copper specimens layout and manufacture for experimental measurements, their further modifications and surface measurements. Further examines the measurement methods, measurement conditions and the experiments of thermal contact resistance.

Theoretical measurements are carried out with the use of models from theoretical part and experimental measurements are carried out with the use of test chamber. Measurements are compared. Based on the results from measurements the conclusions are made, that will be used in the future for space component development.

Abstrakt

Bakalárska práca rieši tepelné prechodové odpory rovinných povrchov v kontakte pre účely projektu tepelného spínača. Zameriava sa hľadanie vhodného matematického modelu na predikciu tepelných prechodových odporov ako možného riešenia pre optimalizáciu tepelného spínača. Práca sa skladá z teoretickej a praktickej časti.

Teoretická časť stručne uvádza pozadie projektu a dôvod vzniku tejto práce. Ďalej rieši ako sú tepelné prechodové opdory definované a faktory, ktoré ich ovlivňujú. Následne uvádza prehľad existujúcich modelov na predikciu tepelných prechodových odporov, vhodnú selekciu modelov pre možné použitie a ich popis.

Praktická časť sa zaoberá návrhom a výrobou medených vzoriek pre experimentálne merania, ich následnými úpravami a povrchovými meraniami. Ďalej rieši spôsoby merania, podmienky merania a samotné merania tepelných prechodových odporov.

Za použitia modelov z teoretickej časti sú vykonané teoretické merania a za použitia testovacej komory experimentálne merania. Merania sú navzájom porovnané. Na základe výsledkov z meraní sú urobené úsudky, ktoré budú požité v budúcnosti pri vývoji vesmírnych komponentov.

Keywords

Thermal contact resistance, thermal contact conductance, thermal conductivity, heat transfer path, vacuum, model, conforming rough surface, miniaturized heat switch, bread board, copper specimen, test chamber, surface parameters, planar surface, contact pressure, interstitial gap

Kľúčové slová

Tepelný kontaktný odpor, tepelná kontaktná vodivosť, tepelná vodivosť, cesta prenosu tepla, vákuum, model, konformne drsný povrch, miniaturný tepelný spínač, bread board, medená vzorka, testovacia komora, parametere povrchu, rovinný povrch, kontaktný tlak, intersticiálna medzera

Rozšírený abstrakt

V roku 2015, bol Letecký Ústav, na Vysokom Učení Technickom v Brně poverený spoločnosťou Arescosmo otestovať "Bread Boardy" (vývojové fázy súčiastky) kozmického spínača vyvíjaného pre Európsku vesmírnu agentúru (ESA).

Kozmický spínač (alebo miniaturný tepelný spínač) je zariadenie schopné regulovane odvádzať teplo z komponentu do vonkajšieho prostredia, ktoré v tomto prípade predstavuje otvorený vesmír a teda vákuum. Zmyslom regulácie je uchovať energiu v družici (alebo inom stroji) alebo naopak odviesť ju preč v prípade jej prebytku a prehrievania družice. Reguláciu zaručuje spínací mechanizmus, ktorý sa pri určitej teplote roztiahne a dostane do kontaktu s proti rozhraním, s ktorým nie je pevne spojený. V tom momente sa vytvorí cesta pre odvod tepla. Keď teplota klesne, mechanizmus sa stiahne a kontakt s protirozhraním zanikne.

Bolo zistené že Bread Boardy nefungujú ako by mali, predovšetkým kvôli zlým kontaktom v konštrukcii, ktoré spôsobovali vysoký tepelný kontaktný odpor respektíve nízku tepelnú kontaktnú vodivosť. Od vtedy začali prípravy tretieho Bread Boardu, pričom jedným z cieľov je optimalizovať tepelné kontaktné odpory za účelom vyriešiť problém nízkej vodivosti. To sa stalo impulzom k vzniku tejto práce, ktorá predstavuje prvý krok v optimalizácii tepelných kontaktných odporov v kozmickom spínači. Prvým krokom je popísať tepelné kontaktné odpory a nájsť vhodný matematický model na predikciu odporov vzájomným porovnaním experimentálnych a teoretických meraní.

Preto tepelný prechodový odpor je definovaný a faktory na ktorých závisí sú popísané. Hlavnými faktormi sú: povrchové parametre, tepelná vodivosť, kontaktný tlak, tvrdosť a intersticiálna medzera. Ďalej, podmienky pre ktoré sú modely testované sú špecifikované, pričom bol braný zreteľ na požiadavky kozmického spínača.

Obecne existuje mnoho modelov ktoré tepelný prechodový odpor opisujú. Preto je urobený prieskum modelov a následne sú vyselektované vhodné modely. Sedem modelov je vybraných pre účely tejto práce.

Na základe znalostí o tepelných kontaktných odporoch a požiadavkách, sú navrhnuté a vyrobené vzorky z medi. Bolo vyrobených pätnásť vzorkov. Dvánasť o priemere 50 mm a tri o priemere 25 mm. Všetky vzorky majú rovnakú menovitú drsnosť Ra 3,2. Vzorky sa majú okrem plochy líšiť aj v drsnosti, kvôli tomu aby bolo možné urobiť experimentálne merania pre rôzne kontaktné tlaky a rôzne drsnosti, tým pádom porovnať modely pri rôznych vlastnostiach kontaktu. Preto boli dodatočne tri väčšie vzorky zbrúsené na menovitú drsnosť Ra 0,25.

Dodatočne boli tiež namerané povrchové parametre, pripravili sa tepelné izolácie na boky vzorkov a boli opísané metódy vyhodnocovania výsledkov. Na základe meraní vlnitosti sa usúdilo že vzorky sú konformne drsné a teda dostatočné ploché, čo umožňuje aplikovať modely pre ploché povrchy. Mimo toho sa zistilo že namerané parametre sa výrazne líšia použitím iných noriem, meracích prístrojov či software-ov, čo môže spôsobiť nepresnosti pri ďalších meraniach. Následne sa špecifikovali podmienky pri ktorých merania prebehnú a vytvoril sa plán meraní.

Šesť naplánovaných meraní prebehlo. Experimentálne merania boli vykonané v testovacej vákuovej komore, ktorá simuluje rozhrania, medzi ktorými sa teplo prenáša.

Hlavným cieľom meraní bolo porovnať teoretické a experimentálne výsledky a na základe toho vybrať vhodný model. Avšak ani jeden z modelov nepredikoval tepelný kontaktný odpor správne. Jedinou výnimkou bol Shlykov-Ganin model, ktorý pri jednom z meraní sedel s experimentálnym meraním. Avšak tento výsledok sa považuje iba za náhodu. Vo výsledku nebol nájdený vhodný model.

Mimo hlavného cieľu však výsledky ukázali že pri zmene kontaktného tlaku pri konštantnom zaťažení tepelný kontaktný odpor vzrastá napriek tomu, že je nepriamo úmerný tepelnej kontaktnej vodivosti, ktorá pri zvyšujúcom kontaktnom tlaku podľa teórie vzrastá.

Z meraní vzorkov o rôznej drsnosti pri jednom porovnaní vyšlo, že pri jemnejšom povrchu tepelný kontakntý odpor klesá, čo sedí z teóriou. Pri druhom porovnaní iných meraní vyšiel opak. To však nekorešponduje s teóriou. No neskôr sa zistilo, že v meraní s jemnejšími povrchmi bola použitá vzorka, ktorá vykazovala odchylky od rovinnosti, čo pravdepodobne zapríčinilo zlé dolahnutie kontaktov a následne vyšší odpor. Preto výsledky, ktoré ukázali vzrast odporu pri jemnejšom povrchu nie sú považované za relevantné.

Porovnanie meraní so vzorkami o rovnakej menovitej velikosti a drsnosti, ale iným počtom kontaktov, vytvorených vzorkami naukladanými na sebe, ukázalo rovnaké výsledky pre tepelný prechodový odpor. To súhlasí s teóriou. Na základe tohoto merania bolo možné usúdiť, že nezáleží či je na sebe poukladaných 6 vzorkov, alebo 3. Tepelný kontaktný odpor medzi povrchmi vzoriek je totiž stále najvýraznejším oproti odporom materiálu a tepelnými kontaktnými odpormi medzi povrchmi vzoriek a rozhraní medzi ktorými sú vzorky v komore uložené.

Na základe výsledkov sú navrhnuté doporučenia pre budúcu prácu a vývoj vesmírnych komponentov.

Bibliography

MATEÁŠIK, Timko Marek. *Tepelný přechodový odpor plošných kontaktů.* Brno, 2019. Dostupné také z: `https://www.vutbr.cz/studenti/zav-prace/detail/117064`. Bakalářská práce. Vysoké učení technické v Brně, Fakulta strojního inženýrství, Letecký ústav. Vedoucí práce Jakub Mašek.

Declaration of authenticity

I declare that I have elaborated my bachelor‘s thesis on the theme of ”Thermal contact resistance of planar surfaces” independently with the use of technical literature and other sources of information which are all quoted in the thesis and detailed in the list of literature at the end of the thesis.

In Brno on 23. May 2019 Timko Marek Mateášik

Acknowledgement

I would like to thank my family for the support. I would like to express special thanks to my supervisor Ing. Jakub Mašek for his guidance and support and Ing. Matej Harčarík for his assistance.

TABLE OF CONTENTS

1 Introduction

In this work, the terms thermal contact conductance (TCC) and thermal contact resistance (TCR) often refer to the same matter, as they are both closely dependent quantities. However both are defined with equations and in calculations must be considered as different. Also many quantities and terms, mentioned in this work, are in literature differently defined, used, named or marked. Therefore, it is recommended to always find out definitions proposed by authors in every literature in order to prevent any misunderstandings. The original, or similar form (the way they were found in literature) of the equations for thermal contact conductance is rather used in this work.

1.1 Space exploration

Since the ancient times space has been the subject of observers. The desire to explore and examine, as a part of burgeoning knowledge, became the key for rise of civilizations. Through the centuries important discoveries were made. The 20th century was one of the biggest milestones in history of space exploration, because of political situation of World War II and Cold War, which started the space race. For the first time a humans put their machine into orbit, the man left the Earth and set a foot on the Moon. Nowadays, half a century later, space exploration still continues. Many space agencies extend their space programme. It is necessary to improve technology to obtain more knowledge. And then, to use the knowledge to improve technology for further, this time more effective, use. One of such agencies, making progress in space technology and exploration, is the ESA.

1.2 European Space Agency

The European Space Agency (ESA) is an international organisation. It unites mainly European countries. It comprises 22 member countries, e.g. the Czech Republic, Italy, France, etc.. Other countries, e.g. Slovakia, Canada, Malta, etc., participate in projects or have cooperation agreements. ESA uses resources of these countries for collective space programme, and in return shares the benefits brought by space programme. Moreover, ESA cooperates with other space agencies worldwide. [11][9]

1.3 ESA objectives

One of the ESA‘s aims is to keep the European space programme in progress. The programme concentrates on examining the Earth, its environment, our solar system, the universe, as well as on developing satellite-based technologies and services with a use of European industry. The missions that the ESA took part in, are listed in on the ESA‘s official website [10].

For future missions there is a demand for new, more efficient and possibly cheaper technologies. Missions for observing Mars are being prepared, therefore the new technological components under development have to be suitable for Martian conditions as well as outer-space environment. [11]

1.4 ESA-Arescosmo-BUT

ESA commissioned Arescosmo (originally Areosekur), an Italian company, with a task of designing a miniaturised heat switch (MHS). Arescosmo, as the prime contractor of the MHS project, developed two bread boards (BBs) [20].

In 2015, the Institute of Aerospace Engineering, University of Technology in Brno (BUT) joined the task and was commissioned by Arescosmo to test the BBs and to become the secondary contractor. The testing of the BBs included the development of an experimental test facility for space condition‘s simulations [20] and complex tests of MHS samples [22]. A report from testing [22] revealed that the BBs did not work as it had been predicted. Moreover, Arescosmo left the MHS project and BUT took the project over. After signing a contract, BUT will become the primary contractor. The dysfunctional BBs were a step back in the MHS development. Since the BUT has taken over, the new objective of the project is to design a third BB instead of the planned engineering qualification model (EQM).

2 Miniaturized heat switch project

The miniaturized heat switch (MHS) is a device regulating heat transfer between an equipment (of satellite or other probe) and a heat sink, that is in contact with the outer, far cooler environment. Mean of the regulation is to save energy. When the cooling is not necessary, the MHS mechanically separates the inner parts and outer environment, so the path for the heat transfer is aborted. [20]

2.1 MHS requirements and specifications

The end product definition of the MHS is stated in [12]. The heat switch shall be a stand-alone item ready to be mounted between a unit and radiator.

The Miniaturized heat switch shall consist of:

a. Hot mounting interface.
b. Cold mounting interface.
c. Switching device to vary the thermal conductance between the hot and cold interfaces.

In the ESA's statement of work [12], all general requirements for the MHS are stated. The Most important requirements for this work are:

Table 1: MHS requirements (important for this work).

Functional and Performance requirements	
Spec. Reference	Description
FPR1	The Heat Switch shall have a peak conductance value greater than 1 W/K.
FPR3	The Heat Switch shall operate in vacuum and in 10 mbar of CO_2.
FPR4	The variable conductivity range of the Heat Switch shall be between 15 C to 25 C of the hot interface.
FPR5	The Heat Switch shall be designed to transport 1 W to 10 W in closed/on mode from the hot interface to the cold interface. When transferring 10 W, the maximum delta temperature in steady state condition shall be 10 K.
FPR6	The Heat Switch shall have a temperature stability of +/- 1 C with a constant power input and constant sink temperature.
Interface requirements	
Spec. Reference	Description
IR1	The Heat Switch shall have a flat mechanical interface on the Hot and Cold side for mounting onto the dissipating component and to temperature sink.
IR2	The Heat Switch shall have a hot mounting surface area of roughly 16 cm^2.
IR3	The Heat Switch shall meet the requirements with cold interface temperatures between -125 C and 50 C and with hot interface temperatures between -55 C and 60 C.

Additional requirements [20] were then specified by Arescosmo:

> The MHS shall not require any electrical power to be activated.
> There shall be no maintenance required to any component of the MHS over the duration of the ground lifecycle.

2.2 MHS components

The basic components of the actual MHS assembly in this work are: hot interface (HI),cold interface (CI), actuator, conductive cover, insulators and copper plates.

The equipment, which needs to be cooled down is mounted on the HI and the external heat sink in the space environment is mounted on the CI. In simplicity the HI can represent the equipment and the CI the space environment. When the HI reaches the determined temperature, it is required that the actuator provides connection between the HI and CI, so that heat is allowed to be transferred out and the important equipment will not overheat. When temperature decreases below the determined value, the actuator must detach the CI from the HI. The MHS must be able to handle the opening and closing of heat transfer path repeatedly.

The actuator is fixed to the HI and strokes in the CI direction. A phase change material (PCM) filled in the actuator, subjected at temperature variation, causes the stroke. This is the principle of switching mechanism.

The conductive cover component is flexible and capable of elastic stroke as a part of the actuator. It is fixed to the HI together with the actuator. Its function is to connect the HI and the CI due to a stroke, in order to create the path for a heat transfer. When the path is created, the MHS is in ON position. When the path is aborted, the MHS is in OFF position.

Three insulators connect the CI and the HI, however they do not allow to transfer the heat, because of their very low thermal conductivity. The insulators, the CI and the HI are structural parts of the MHS.

The copper plates are additionally mounted on both interfaces of the MHS in order to improve a stiffness of the MHS during the transportation on the Earth. [20]

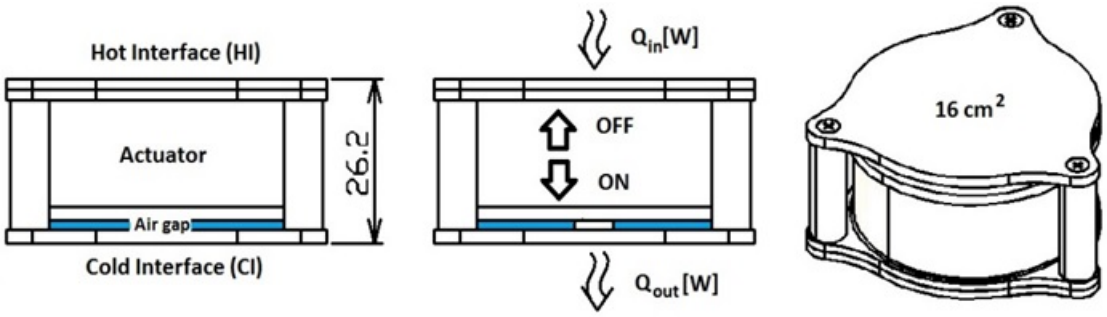

Figure 1: Switching phase of MHS when thermal load is applied. [21]

2.3 Bread boards design and tests

Until now, as already mentioned, two BBs were manufactured and tested. One BB has stroke 1,5 mm and is filled with parraffin C15/C16 PCM, which has melting temperature 13,5 °C. The second BB has stroke 1,7 mm and is filled with parraffin C16 PCM, which has melting temperature 18 °C. Basic dimensions of the MHS design are following:

$D_S = 42\,\text{mm}$	Diameter.
$H_S = 26,2\,\text{mm}$	Height.
$A_S = 1546,53\,\text{mm}^2$	Area of the MHS thermal loaded surface.
$D_P = 56\,\text{mm}$	Diameter.
$H_P = 8\,\text{mm}$	Height.
$A_P = 2463\,\text{mm}^2$	Area of the plate.
$H = 42,2\,\text{mm}$	Height.

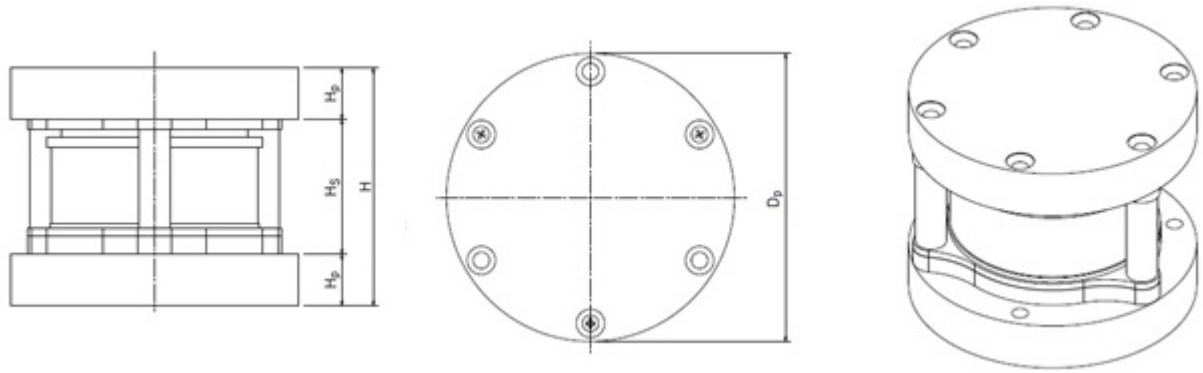

Figure 2: MHS assembly (MHS between additional copper plates). [20]

The BB tests revealed serious shortcomings. Both BB's thermal conductance was approximately five times lower than required when measured in ON position. The investigation led to the conclusion, that poor thermal conductivity was mainly caused by poor contact surfaces quality in the MHS and conductive cover, of which thermal conductivity was measured to be about ten times lower than expected. Other aspects also had their influence on low thermal conductivity, but they are not important for this work. Thus they are not mentioned. [22]

2.4 Recent objectives

A new, third BB is currently in development. Based on the conclusions from the extensive testing, it has been assumed that further research in heat transfer through contact has to be done. From this assumption originates the purpose of this work, that concerns with a problem of thermal contact conductance (TCC), its dependent quantity thermal contact resistance (TCR) and available solution for optimization.

To optimize the heat transfer in the MHS by reducing the TCR (increasing the TCC) could lead to results, that would meet the MHS requirements stated in Chapter 2.1.

This work consists of a theoretical and practical part. The theoretical part examines what the TCR is, how it works, what factors it depends on and how to calculate it. The

practical part, based on assumptions made in the theoretical part examines the TCR experimentally on designed specimens and compares the results with theory.

Thus the objectives are as follows:

- To define the TCR.
- To describe the factors the TCR depends on.
- To review and select the appropriate models for TCR (or the TCC) prediction, including theoretical models and correlations.
- To design and manufacture the specimens, based on theoretical assumptions.
- To make calculations of the TCR prediction based on selected models.
- To carry out an experiments with designed specimens.
- To compare the experimentally obtained values of the TCR with the predicted ones.
- To find the most suitable model for the TCR prediction.

The objectives can be summarized by two main goals. To understand the TCR and to find the most suitable model for its prediction. It is an important part of the solution for the TCR reduction in the MHS. The acquired knowledge can be further used in the third BB design.

3 Thermal resistance

3.1 Thermal path in the MHS

Between the components of the MHS, many contacts occur. Every contact acts resistively for a heat flow, what occurs as a temperature jump in temperature-thickness dependence. This is an effect of the TCR, caused by contact imperfections. This effect can be seen in Figure 3. Not only the contacts, but solids too, act resistively. In comparison with contact, it is less significant but surely not negligible. Thermal path in the MHS can be represented as thermal circuit with thermal resistors. The resistors, generally marked only as R, represent thermal resistance or TCR component in circuit. The thermal path in MHS can be substituted by schematic circuit with resistors. The circuit can be seen in Figure 4. The contacts are marked with "c" index. The most significant contact is between the actuator and the CI when the actuator is in ON position, the contact $R13c$. All the heat is transferred through it.

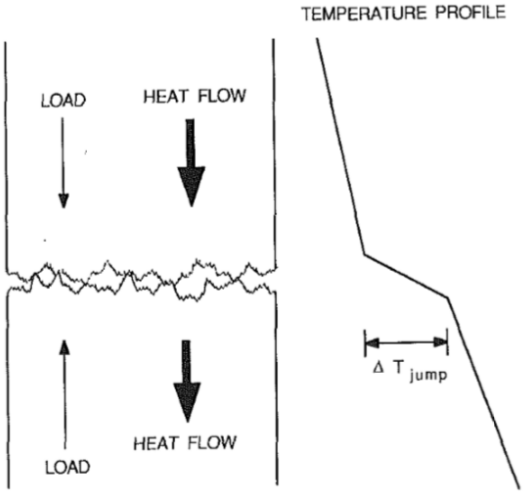

Figure 3: Heat conduction across two rough surfaces in contact. [18]

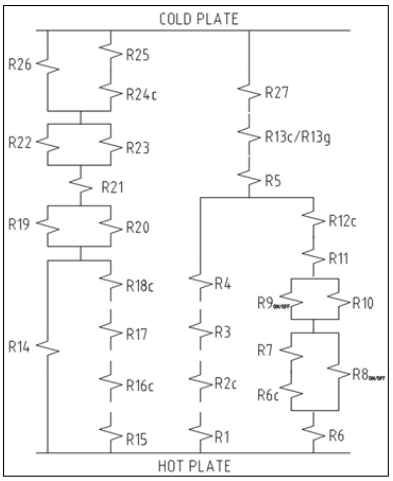

Figure 4: The circuit of thermal resistances in MHS.

For the purposes of the MHS development, the effect of TCR is ineligible as one of the ways of achieving higher efficiency in heat transfer by reducing the TCR.
Best option for dealing with the TCR would be to design an ideal contact. However, in engineering applications no ideal contact between two solid surfaces exists.
It is always necessary to consider contact imperfections to understand why and how the TCR affects the heat flow.

3.2 Thermal conduction in solid

Equation for heat tranfer rate or heat flow rate through solid due to thermal conduction is given as:

$$Q = \frac{kA\Delta T}{t} \qquad [W] \tag{1}$$

where Q is function of area A [m^2] through which the heat transfers, temperature difference ΔT [K] on the opposite sides of solid with thickness t [m] and material thermal conductivity k [W/mK].

Thermal conductivity of material k is physical property. It is an ability of the material to transfer the heat due to conduction. This property is the function of temperature, however, for narrow range of temperature differences it is considered to be constant. The higher the thermal conductivity, the higher the heat flow is. Thermal conductance K is basically thermal conductivity k referenced to actual dimensions of the solid. It is obtained by the equation:

$$K = \frac{kA}{t} = \frac{Q}{\Delta T} \qquad \left[\frac{W}{K}\right] \tag{2}$$

Thermal resistance R is reciprocal value of K.

$$R = \frac{1}{K} = \frac{t}{kA} \qquad \left[\frac{K}{W}\right] \tag{3}$$

3.3 Thermal conduction in contact

Thermal conduction in contact refers to heat transfer through the contact established between two solids. In real contact, only some spots of actual surfaces are in contact. Between the remainder, the gap is present. The gap allows the heat to transfer due to convection and radiation, too. Thus the total heat passing through the contact is the sum of all three basic mechanisms of heat transfer and can be expressed by equation:

$$Q_{total} = Q_{conduction} + Q_{convection} + Q_{radiation} \qquad [W] \tag{4}$$

For better understanding of thermal conduction in contact, more convenient form is proposed:

$$Q_c = Q_s + Q_g + Q_r \tag{5}$$

where the total heat transfer rate is understood as thermal conduction in contact Q_c, which is the sum of the heat transfer rate through the solid spot Q_s, the gap Q_g and due to radiation Q_r. Therefore, the TCC can be expressed as:

$$h_c = h_s + h_g + h_r \qquad \left[\frac{W}{m^2K}\right] \tag{6}$$

Where radiation component can be neglected for applications under 600 °C [41] and so the expression is:

$$h_c = h_s + h_g \tag{7}$$

To obtain the TCC referenced to actual dimension of the area A in contact, the following equation is used:

$$K = h_c A \qquad \left[\frac{W}{K}\right] \tag{8}$$

And the TCR is reciprocal to the TCC referenced to the actual contact area[1]:

$$R = \frac{1}{K} = \frac{1}{h_c A} \qquad \left[\frac{K}{W}\right] \tag{9}$$

[1]In literature, TCR R can be also found to be directly reciprocal to TCC, $R = \frac{1}{h_c}$. Although this definition will not be used in this work.

For contact between two solids heat flow rate is:

$$Q_c = h_c A \Delta T = \frac{\Delta T}{R} \tag{10}$$

The equations in this Chapter and Chapter 3.2, are generally available in scientific literature of heat transfer and TCR research, e.g. [26] and [41].

Note: The symbol "R" is used for both, thermal resistance in solid (Chapter 3.2) and TCR, as it is property obtainable for both, solid and contact. If R is obtained for solid, it represents the thermal resistance of solid and if it is obtained for contact it represents the thermal resistance in contact (also called TCR). The relationships (3) and (10) differs, but it still generally represents thermal resistance. Thermal resistance in this form can be further used in calculations in circuit, where both solids and contacts are present. The same applies to thermal conductance "K".

3.4 TCC factors

The magnitude of the TCC is dependent on many different factors, of which the most influencing ones are those stated below. However, even nowadays, it is only roughly known, how exactly these factors influence each other and eventually the TCR.

3.4.1 Surface

No real surface, even a very smooth one, is ever perfectly flat. Heights consisting of peaks, valleys and other irregularities occur in microscopic view. In engineering surfaces, it is mostly a result of a machining tool, surface finishing, or generally any technology the surface undergoes. Geometry, waviness and roughness are basic characteristics of the surface texture.

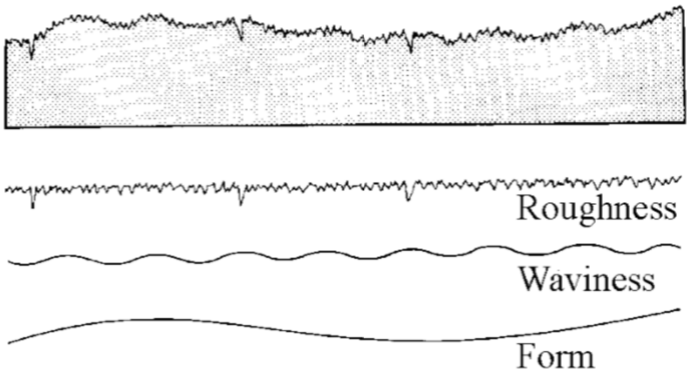

Figure 5: Geometry (form), waviness and roughness as characteristics of the surface texture. [13]

Basic surface geometries in contact are combinations of planar or flat and spherical. One important consideration has been done in the TCC research. Even if the geometry of the surface in contact is considered to be nominally flat and not spherical, it still can differ in flatness. The flatter the surface is, the more uniform distribution of the contact areas (spots) in contact is and the bigger solid spot TCC is. The surface is assumed as

conforming rough when flatness deviation is maximum ten times the surface roughness Ra [33]. Otherwise it is a non-conforming rough surface, which can appear as convex, concave, or simply too wavy curvature of the surface. The fact that the surface is either conforming or not indicates how the spots are distributed along the nominal contact area. In case of the conforming rough surface, the spots are distributed in the whole nominal contact area. In case of the non-conforming rough surface, out of flatness is too big and spots occur only in the contact area smaller than the nominal contact area. Similar or more specific description of surface geometry can be found in the literature, e.g. [4]. In Figure 6 types of surfaces in contact, with spot distribution are shown.

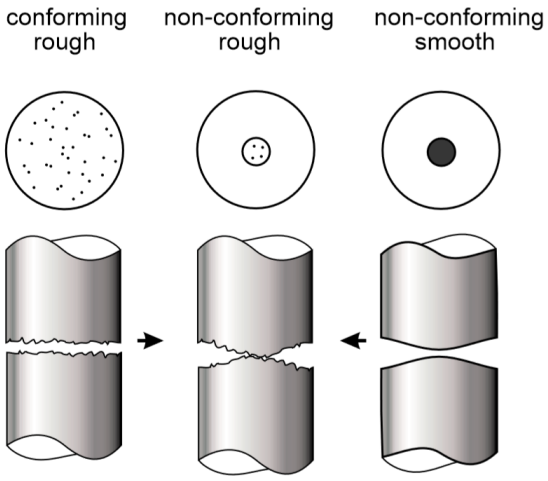

Figure 6: Conforming rough, non-conforming rough and non-conforming smooth contact surfaces with spot distribution. [6]

Waviness is also affecting the TCC and should not be neglected [34]. According to [33], for conforming rough surface the average waviness height w_a [µm] should be maximally four times the roughness Ra. Nevertheless the low-pass and high-pass filters used in waviness measurements were not specified. Therefore appropriate value of waviness can be barely obtained.

Roughness strongly influences the TCC. The actual contact area is created by the highest peaks of the heights, creating the so called spots when surfaces are in contact. Their size and distribution vary in dependence on the roughness. To obtain the accurate size and distribution of all the spots is practically impossible. Therefore, roughness parameters are preferred. The root mean square (RMS) surface roughness (Rq) σ [µm] is one of the engineering parameters used to describe the roughness. Another one, commonly used, is the arithmetic average height (Ra) σ_{Ra} [µm], equal to the center line average (CLA) surface roughness parameter. The effective RMS surface roughness σ_s of the two RMS surface roughnesses σ_1 and σ_2 in contact is:

$$\sigma_s = \sqrt{\sigma_1^2 + \sigma_2^2} \qquad [\mu m] \tag{11}$$

To obtain the RMS roughness from Ra roughness, following equation is used [25]:

$$\sigma = \sqrt{\frac{\pi}{2}}\sigma_{Ra} \approx 1,25\sigma_{Ra} \tag{12}$$

Although, this correlation can be strongly inaccurate. The mean absolute profile slope m [rad] (alternatively marked in literature as: $|tan(\theta)|$, Δa, Rda, $R\Delta a$) is another surface roughness parameter affecting the TCC. The effective mean absolute profile slope m_s of the two surfaces in contact is:

$$m_s = \sqrt{m_1^2 + m_2^2} \qquad [\text{rad}] \tag{13}$$

where m_1 and m_2 are mean absolute profile slopes of the surfaces in contact.

The parameters σ_s and m_s are graphically shown for two surfaces in contact in Figure 7. "Y" is the mean plane separation and will be describe in Chapter 3.4.5.

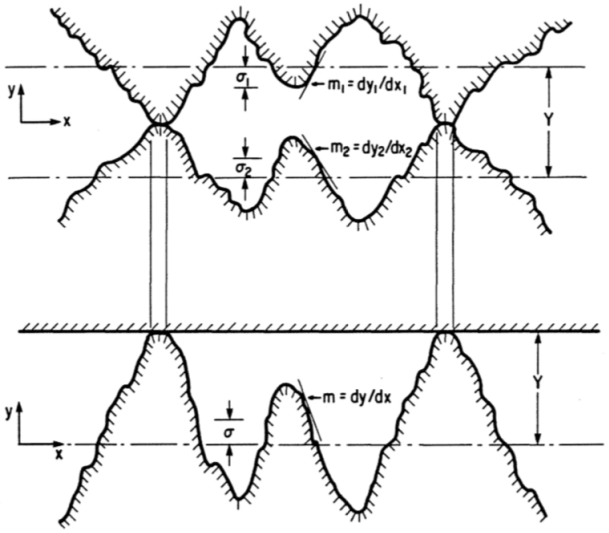

Figure 7: The microscopic view of conforming rough contact. [15]

According to [40] correlation between σ and m is:

$$m = 0,125(\sigma \times 10^6)^{0,402} \qquad [\text{rad}] \tag{14}$$

which is valid in the range:

$$0,216\,\mu\text{m} \leq \sigma \leq 9,6\,\mu\text{m}$$

However this correlation (14) can show a significant error and should be used only when measured values of m are not available. Also in [40] an example of calculation with correlation is proposed where σ is actually not multiplied by 10^6, what makes more sense in respect to actual values. The values of σ must be substituted in [µm]. Article [40] refers to [1], where similar correlations can be found.

Similar to the mean absolute profile slope is the RMS profile slope $m‘$ (alternatively marked in literature as: $\dot{\sigma}$, Δq, Rdq, $R\Delta q$). Analogically to eq.(13), the effective RMS profile slope $m‘_s$ of the two surfaces in contact is:

$$m‘_s = \sqrt{m‘^2_1 + m‘^2_2} \qquad [\text{rad}] \tag{15}$$

To obtain RMS slope from the mean absolute profile slope, following equation (analogically as in eq.(12)) is used [4]:

$$m‘ = \sqrt{\frac{\pi}{2}} m \approx 1,25m \tag{16}$$

Although, this correlation can be strongly inaccurate (as in eq.(12)).

Note: The surface parameters and their definitions are freely available in literature, e.g. [14].

3.4.2 Thermal conductivity

Two solids with thermal conductivities k_1 and k_2 have harmonic mean thermal conductivity k_s where:

$$k_s = \frac{2k_1k_2}{k_1 + k_2} \qquad \left[\frac{W}{mK}\right] \tag{17}$$

With higher value of k_s, the TCC increases.

3.4.3 Contact pressure

The contact pressure between two solids pressees the peaks of the surface asperities against each other and deforms them. Therefore, more spots occur, get bigger and the actual contact area increases proportionally to the contact pressure. The higher the pressure, the higher the TCC is. Pressure in contact P is calculated as:

$$P = \frac{F}{A} \qquad [\text{Pa}] \tag{18}$$

Where F is the force or the load applied on the area A, which is in this case assumed as nominal contact area.

3.4.4 Hardness and Elastic modulus

The resistance of the solid material in contact against the indentation of the second solid due to contact pressure is expressed by the hardness H [Pa] of the softer material. In the TCC research different investigators considered different hardness. Therefore, hardness will be determined specifically in Chapter 4.3 for each selected model.

In some cases (e.g. eq.(26)), instead of hardness, an elastic modulus E [Pa] is used. The equivalent or the effective elastic modulus E' can be calculated as [24]:

$$E' = \left(\frac{1-\mu_1^2}{E_1} + \frac{1-\mu_2^2}{E_2}\right)^{-1} \qquad [\text{Pa}] \tag{19}$$

Where E_1, E_2 are elastic modules of solids in contact and μ_1, μ_2 $[-]$ are Poisson numbers or Poisson‘s ratios of solids in contact.

3.4.5 Interstitial gap

The interstitial gap has an important role in the TCC as the actual contact between solids appears only in some spots and the rest is the bare surface separated by gap. The size of distance between two surfaces in contact or the thickness of the interstitial gap is a result of all the previous factors. It can be described with mean plane separation, also called the effective gap thickness Y [µm] or by relative mean plane separation (called in

literature also as: relative effective gap thickness or dimensionless mean plane separation) λ [37] where:

$$\lambda = \frac{Y}{\sigma_s} \qquad [-] \tag{20}$$

This parameter has an important role in models for the TCC prediction, mostly for gap TCC h_g .

The interstitial gap can be empty or filled. When contact is established in vacuum environment and no interstitial material is added, the gap is simply empty. Thus the heat is transferred only by solid spots and $h_g = 0$. When the gap is filled, it is mostly due to gaseous/fluidic environment such as air, in which contact is established. When gas/fluid is present in the gap, many factors influence the gap TCC and heat transfer becomes far more complex in contrast with contact in vacuum environment.

In an effort to enhance the TCC various interstitial materials can be added. There exist wide variety of interstitial materials or mediums, e.g.: coatings, layers, metallic and non-metallic foils, wire screens, greases, powders, etc..

The principle of all the enhancing interstitial materials is to fully fill up the gap with material of high thermal conductivity and to provide heat transfer through the whole contact area with minimum thermal loss.

3.4.6 Other factors

The main factors have been mentioned and described, however these are not the only ones. It is known that temperature influences many material properties, including hardness, elastic modulus, thermal conductivity, etc., thus indirectly also TCC . It shall be taken into account for specific extreme conditions. In literature , wide variety of less common, specific parameters influencing the TCC are proposed, e.g. a bandwith parameter, variance of surface heights, variance of surface slopes, radius of curvature of summits, fractal dimension number, load exponent, plasticity index, distribution functions, etc.. They are mostly sub-factors of main factors and are often hardly practically obtainable, because of the lack of information in literature. [16]

3.4.7 Investigated conditions

In this work, experimental measurements are focused on the TCC or the TCR of nominally flat, conforming rough surfaces with surface roughness variations of specimens in contact and contact pressure variation. Vacuum conditions at temperatures of contact in range from 0 °C to 60 °C and contact pressure roughly under load of 80 N is suggested. The material of solids shall be chosen in respect to materials used in the MHS BB design or similar ones.

The nominally flat, conforming rough surface is chosen in respect to contacts in construction of MHS (Chapter 2), primary the most crucial one (R13c), which ideally should have the mentioned geometry, if the MHS works properly. Also nominally flat geometry is far more simple for experimental work than spherical one.

Vacuum conditions are chosen for the purpose of elimination heat leaks due to convection

from surfaces in no contact (specimen‘s side surfaces) and better validation of the TCC models by reducing the total TCC to only the solid spot TCC. Separate measurement of the solid spot and gap TCC can make results more accurate, as the possible inaccuracies in both, solid spot and gap TCC, do not merge into one result. Therefore the inaccuracies can be described separately for both. Of course this is invalid when enhancing interstitial media in gap is present. Vacuum eliminates only the effect of gaseous interstitial media. Also, according to the FPR3 requirement (Chapter 2.1, Table 1), the MHS should be able to operate in vacuum, thus simulation of the TCC in vacuum conditions is desirable.

The contact temperature range 0 °C to 60 °C is selected in respect to the HI operational contact temperature range, when MHS is at ON position. 60 °C is the upper limit of the HI required operational contact temperature range, mentioned in Chapter 2.1, 1. Lower limit of 0 °C roughly represents the temperature at which the PCM begins to change its phase.

The contact load is chosen in respect to capabilities and limitations of test chamber [20] and shall stay constant throughout all the experiments. The pressure in contact under constant load can differ with nominal area, but shall stay constant when roughness variation is compared. The variation of contact pressure allows to find the appropriate TCC models in wider spectrum of dependent factors.

The materials used in MHS BBs or similar are in preference, as it is the most effective way how to simulate the actual TCC in MHS. These materials are mostly metals with relatively high thermal conductivity.

Another variable parameter in tests is the surface roughness and parameters dependent on it. The surface roughness parameter is probably the most modifiable TCC parameter in the actual MHS construction and as mentioned in Chapter 2.3, one of the reasons of low thermal conductivity of two BBs is poor surface quality. Therefore, the investigation of surface roughness effect and its varieties on TCC is of primary importance.

The experimental conditions and specimen specifications will be described in detail later, in Chapter 6.1.1.

4 Thermal contact conductance models

The review of the TCC models in literature has been summarized. The appropriate models for comparison with experiments were selected. Every selected model is briefly described.

4.1 Review

Research on Theoretical prediction of the TCC is reviewed in [3, 4, 17, 36, 37, 41] The model for TCC prediction can be understood as theoretical model or as correlation, which is often derived from a theoretical model. Unlike the correlation, a theoretical model has more complex form, based on many assumptions and derivations, while the correlation is usually in more convenient form for calculations. Correlation does not even have to be derived from theoretical model, but can be estimated directly from experimental measurement. Most theoretical models and correlations for the TCC are compendiously reviewed in [16], mainly for the solid spot TCC and in [27] mainly for the gap TCC. Theoretical models can be further divided according to deformation the surfaces undergo, as plastic, elastic and elasto-plastic. The in-depth review and comparison of elastic and plastic theoretical models is in [32]. An example of elasto-plastic model is in [30]. The enhancement methods of the TCC are reviewed in [27] [17]. The characteristic for theoretical models is also different assumption of asperity distribution on the surface. Gaussian type is most common. Other distribution types, such as random, fractal or modified gaussian can be found in literature. The types of distribution influence the final form of models, in which they are presented.

Despite all the theoretical models and correlations, no general model exists. The existing models often have only a narrow range of applicability. It mainly depends on theoretical considerations for which the TCC factors and experimental conditions the models were developed and verified.

4.2 Selection

Not every proposed model is appropriate for use in this work. Thus only few models have been chosen for comparison with experiments. The selection requirements are:

1. Model must consider and be usable for nominally flat contact surface. This work is focused on nominally flat conforming rough surfaces. However, not all the models differ between conforming or non-conforming rough surface and assume the surface only as flat. Therefore, these models can also fit for the TCC prediction of conforming rough surface.

2. All the models‘ parameters must be described and calculable. The reason for this requirement is mathematical complexity and disarrangement of many mathematical prescriptions. Derivations of equations are often missing, variety of terms are used for the same parameters in different articles, moreover the same model can be found using different parameters without explanation. Overall, it is complicated to find proper, comprehensible models among all the models in literature, but only those can be selected for further use.

3. All the dependent factors, especially those mentioned in Chapter 3.4, have to be

the commonly available or obtainable engineering parameters. Not all the parameters are easy to obtain practically, even if they are defined. For the TCC prediction it is an advantage to use the parameters the values of which can be found in literature or can be measured conventionally. Then, the predictions are effective, require fewer additional measurements as the parameters are normalized or given directly from the manufacture process and necessary measurements can be easily done.
One example of the rare parameter is contact microhardness, which requires more extensive measurements. This parameter will be mentioned in Chapter 4.3.3.

4. A Model must not require any additional estimation of correlation constants. Prediction of TCC must be possible without the existence of real components (specimens).

5. A Model must not require any specific topic-related software use including additional programming.

4.3 Theoretical Models and Correlations

The selected models are briefly listed in Table 2 and then described separately in chapters. Even if the models have their range of applicability different from the investigated conditions in this work (Chapter 3.4.7), it is not considered as a problem. It is so, because models can actually be applicable also for conditions they were not developed, verified or considered for. The unexamined spectrum of the TCC research is still wide.

Table 2: Selected TCC models and their basic description

Models			
Theoretical models	Chapter	Description	Tested material
Cooper-Mikic--Yovanovich (CMY)	4.3.1	plastic deformation; one correlation; gaussian distribution	stainless steel*; aluminum*
Mikic	4.3.2	elastic deformation; derived from CMY model; three correlations; gaussian distribution	stainless steel*; aluminum*
Yovanovich	4.3.3	plastic deformation; reccoralted CMY model; improved and extended; gaussian distribution	stainless steel*; aluminum*
Correlations	Chapter	Description	Tested material
Tien	4.4.1	developed for similar metals in contact	stainless steel; aluminum
Shykov-Ganin	4.4.2	mean radius of contact spot $a_s = 30$; no slope considered	copper; steel; aluminum; nickel; uranium
Malkov	4.4.3	mean radius of contact spot $a_s = 40$; no slope considered	stainless steel; molybdenum
Mikic-Rohsenow	4.4.4	developed for similar metals in contact	stainless steel

* It is concluded by the author that most probably these materials were used.

4.3.1 Cooper-Mikic-Yovanovich model

One of the earliest of TCC models was theoretical model called Cooper-Mikic-Yovanovich (CMY) [5]. The CMY model considers plastic deformation, gaussian height distribution of surface asperities (profile and slopes), isotropic surface and random distribution of the asperities in contact area. CMY theoretical model is:

$$h_s = \frac{\sqrt{2}k_s}{4\sqrt{\pi}}\frac{m_s}{\sigma}\frac{exp(-\lambda^2/2)}{(1-\sqrt{0,5erfc(\lambda/\sqrt{2})})^{1,5}} \tag{21}$$

$$\lambda = \sqrt{2}erfc^{-1}(2P/H) \tag{22}$$

and the resulting correlation:

$$h_s = 1,45\frac{k_s m_s}{\sigma}\left(\frac{P}{H}\right)^{0,985} \tag{23}$$

that is valid for ranges:

$$3,6\times10^{-4} \leq \left(\frac{P}{H}\right) \leq 1\times10^{-2}$$
$$1\,\mu m \leq \sigma \leq 8\,\mu m$$
$$0,08 \leq m \leq 0,16$$

H is microhardness of the softer material, however the type is not specified in original paper. In [31] microhardness is proposed to be three times the yield stress or flow stress S_y [Pa]:

$$H = 3S_y \tag{24}$$

4.3.2 Mikic model

Mikic [24] developed an elastic model based on the CMY model with consideration of an elastic contact area to be half the plastic contact area. The Mikic model is:

$$h_s = \frac{k_s}{4\sqrt{\pi}}\frac{m_s}{\sigma}\frac{exp(-\lambda^2/2)}{(1-\sqrt{0,25erfc(\lambda/\sqrt{2})})^{1,5}} \tag{25}$$

$$\lambda = \sqrt{2}erfc^{-1}(4\sqrt{2}P/(E'm_s)) \tag{26}$$

The correlation for pure elastic deformation is:

$$h_s = 1,55\frac{k_s m_s}{\sigma}(\sqrt{2}P/(E'm_s))^{0,94} \tag{27}$$

He also developed a correlation for pure plastic deformation:

$$h_s = 1,13\frac{k_s m_s}{\sigma}(P/H)^{0,94} \tag{28}$$

And correlation suitable for larger loads, assuming plastic deformation of the asperities and elastic deformation of the substrate:

$$h_s = 1,13\frac{k_s m_s}{\sigma}(P/(H+P))^{0,94} \tag{29}$$

The type of deformation depends on value of deformation parameter γ where:

$$\gamma = \frac{H}{E'm_s} \qquad [-] \tag{30}$$

If $\gamma \geq 3$ then deformation is predominantly elastic and when $\gamma \leq 0,33$ deformation is predominantly plastic. H microhardness is assumed to be the same as in eq. (24).

4.3.3 Yovanovich model

The CMY theoretical model was re-correlated in 1981 by Yovanovich [38] (it can be found also in the article from 1982 [39]) with expression:

$$h_s = 1,25\frac{k_s m_s}{\sigma}\left(\frac{P}{H}\right)^{0,95} \tag{31}$$

valid in the range:

$$10^{-6} \leq \frac{P}{H} \leq 2,2 \times 10^{-2}$$

Relative mean plane separation λ was approximated by expression [38]:

$$\lambda = 1,184[-ln(3,132\frac{P}{H})]^{0,547} \tag{32}$$

Another approximation proposed in 1988, is:

$$\lambda = 1,363[-ln(5,589\frac{P}{H})]^{0,5} \tag{33}$$

And one more power law approximation [2]:

$$\lambda = 1,53[-ln(3,132\frac{P}{H})]^{-0,097} \tag{34}$$

Hardness H is assumed to be three times the yield stress of the softer material in contact. Eq.(24) is used.

In 1985, Hegazy [15], using Yovanovich's correlations [38], investigated the more appropriate hardness. His investigation revealed that surface microhardness varies in dependence not only on the surface material type but also on the machining process. Relationship for appropriate microhardness is:

$$H_c = c_1\left(0,95\frac{\sigma}{m}\right)^{c_2} \qquad \text{[GPa]} \tag{35}$$

Where H_c is the contact microhardness. c_1 andc_2 are coefficients obtained from Vickers microhardness dependency on indentation depth and are related to Brinell and Rockwell hardness. Another relationship is:

$$H_c = (12,2 - 3,54H_B)\left(\frac{\sigma}{m}\right)^{-0,26} \qquad \text{[GPa]} \tag{36}$$

Where Brinell hardness H_B and contact microhardness H_c are in GPa. Both correlations are based on Vickers microhardness tests and developed for four specific metals, but can be used for wide range of metals. Thus the correlations are only semi-general. Later, Song and Yovanovich [29] developed the relationship:

$$\frac{P}{H_c} = \left(\frac{P}{1,62c_1(\sigma/\sigma_0 m_s)^{c_2}}\right)^{1/(1+0,071c_2)} \tag{37}$$

Where $\sigma_0 = 1\mu m$. This correlation can be also used for wide range of metals. In 1996, Sridhar and Yovanovich [31] made a relationship for coefficients c_1 and c_2:

$$c_1 = 4 - 5,77\frac{H_B}{3178} + 4\left(\frac{H_B}{3178}\right)^2 - 0,61\left(\frac{H_B}{3178}\right)^3 \qquad [-] \tag{38}$$

$$c_2 = -0,37 + 0,422 \left(\frac{H_B}{c_1} \right) \qquad [-] \tag{39}$$

valid for range:

$$1300\,\text{MPa} \leq H_B \leq 7600\,\text{MPa}$$

Only the values of H_B in MPa must be substituted into these correlations.

4.4 Correlations

4.4.1 Tien

Tien [35] proposed correlation:

$$h_s = 0,55 \frac{k_s m`_s}{\sigma} \left(\frac{P}{H} \right)^{0,85} \tag{40}$$

Hardness H is is obtained the same as in eq. (24). However, it is unclear to which material in contact the proposed hardness refers, probably because Tien developed correlation (40) for similar metals in contact. In this work only the same materials in contact are used. Therefore it does not matter which one is used. For contact of dissimilar metals, right estimation of hardness has to be considered. Correlation was developed for stainless steel and aluminium.

4.4.2 Shlykov-Ganin

Shlykov and Ganin [28] proposed correlation:

$$h_s = 2,1 \times 10^4 k_s \left(\frac{P}{H} \right) \tag{41}$$

$$H = 3S_u \tag{42}$$

and for metals with high degree of cold work:

$$H = 5S_u \tag{43}$$

Where S_u [Pa] is the ultimate strength of the less plastic metal. Considered as the one with lower value of S_u. Shlykov and Ganin assumed the mean radius of contact spot a_s equal to 30 µm, which is already included in eq.(41). Correlation was developed for copper, steel, aluminium, nickel and uranium. The vacuum pressure was 0,013 Pa.

4.4.3 Malkov

Malkov [19] proposed correlation:

$$h_s = 0,118 \frac{k_s}{a_s} \left(C \frac{P}{H} \right)^{0,66} \tag{44}$$

Where assumed mean radius of contact spot a_s is equal to 40 µm, and thus the correlation (44) can be rewritten as:

$$h_s = 2,95 \times 10^3 k \left(C \frac{P}{H} \right)^{0,66} \tag{45}$$

$$C = 1 \text{ for } \sigma_{1,Ra} + \sigma_{2,Ra} \geq 30\,\mu\text{m}$$
$$C = [30/\sigma_{1,Ra} + \sigma_{2,Ra}]^{1/3} \text{ for } 10\,\mu\text{m} \leq \sigma_{1,Ra} + \sigma_{2,Ra} < 30\,\mu\text{m}$$
$$C = 15/\sigma_{1,Ra} + \sigma_{2,Ra} \text{ for } \sigma_{1,Ra} + \sigma_{2,Ra} \leq 10\,\mu\text{m}$$

$$2 \times 10^{-4} \leq CP/H \leq 8 \times 10^{-3}$$

Hardness H is obtained by eq.(42), where S_u is ultimate strength of material with less strength. The correlation was developed for ground, turned and lapped stainless steel and molybdenum. The temperature in the contact zone varied from 250 °C to 520 °C and vacuum pressure was 0,013 Pa.

4.4.4 Mikic-Rohsenow

Mikic and Rohsenow [25] proposed the correlation:

$$h_s = 0,9\frac{k_s m}{\sigma}\left(\frac{P}{H}\right)^{16/17} \tag{46}$$

$$0,896\,\text{MPa} \leq P \leq 103,4\,\text{MPa}$$

where m is the larger of the two slopes (m_1, m_2) and H is Vickers or Knoop microhardness. Similarly as in Tien correlation (40), it is no clear to which material in contact the hardness refers. Only the same materials in contact are used in this work, thus it does not matter which one is chosen, however the right estimation of hardness has to be considered in contact of different materials. The correlation was developed for stainless steel and vacuum pressure 0,0067 Pa.

5 Specimen layout

For the experimental investigation of the TCR, the specimens have to be designed and manufactured. Before the specimens are manufactured the investigated conditions and MHS requirements has to be considered including the manufacture process itself. The Conditions, the specimens will be tested in, are stated in Chapter 3.4.7.

In this Chapter, specimen specifications, their further preparations for measurements and the TCR evaluation method, including multiplying effect, are described.

How are the specimens going to be tested and the evaluation of TCR from experimental data is more extensively explained in Chapter 6. For testing the test chamber is used, that is briefly described in Chapter 6.3.1. The specifications and development of test chamber are stated in [20].

5.1 Specimen specifications

The specimens are designed to be made from 99,9 % pure copper (EN CW004A/ Cu-ETP) with a cylindrical body with thickness of 5 mm and diameter of 50 mm or 25 mm. The roughness Ra of all the specimens is prescribed to be 3,2 µm. Fifteen specimens were manufactured by a wire-cutting method. Three specimens have diameter of 25 mm and twelve of diameter 50 mm. All the specimens have drilled hole in center with diameter of 6 mm and two half-radiuses of 3 mm on the sides. The thermal conductivity of pure copper is considered to be 390 W/mK.

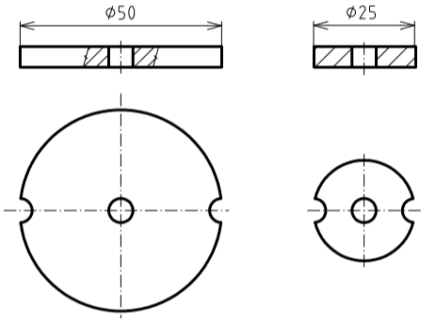

Figure 8: Designed copper specimens.

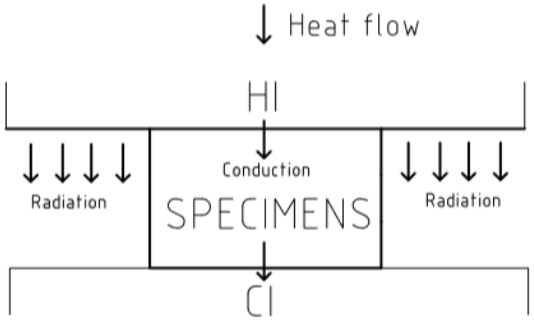

Figure 9: Smaller specimens between interfaces.

The designed specimens can be seen in Figure 8. The mechanical drawings can be found in Appendix, Figures 18 and 19. The manufactured specimens are shown in Appendix, Figures20, 21, 23 and 22.

Copper is one of the materials used in MHS and has high thermal conductivity, which makes thermal properties more significant. Thus, copper is chosen as specimen material.

Diameters are chosen in respect to capabilities of test chamber, where HI and CI have similar contact area as larger specimens. Use of whole area as contact area is important, because otherwise heat can leak due to radiation and can make measurements inaccurate.

Heat leakage is ineligible. However, it is not known how big the leakage due to radiation actually is. Therefore both the specimens with larger and smaller diameter were designed for comparison. The potential area where heat could leak due to radiation can bes seen in Figure 9. If the heat leakage due to radiation through the area in no contact (in case when smaller specimens were used) is negligible, smaller specimens could be further used in future measurements. This would save the amount of material used for specimens. Another reason for diameter variety is to compare different contact pressures (Chapter 3.4.7).

Thickness of 5 mm allows to put six specimens on each other between the HI and CI, creating stack. The more about stack and the contact multiplying effect is in Chapter 5.3 and Chapter 5.3.1. Space between HI and CI in test chamber is roughly 30 mm. Thickness of 5 mm was also chosen as appropriate minimal thickness for manipulation.

Function of holes in the centre is to connect the amount of specimens into one stack. Connection material is Torlon, shaped into simple dowel (Appendix, Figure 35), which centers the specimens and makes the contact areas to lay on each other with whole contact are. Torlon is material with very low, negligible thermal conductivity. Torlon dowels must be made for all the varieties of stack, except the stack with one specimen. Radiuses on the sides have gripping function in order of further manipulations, which will be considered in Chapter 5.2.1.

Roughness of 3,2 µm is roughly the roughness created by wire-cutting process and could not be optimized. The exact values of Ra were measured in manufacture and are listed in Table 3 for specimens with diameter of 50 mm and 4 for specimens with diameter of 25 mm. Both tables include information about marking of specimen, both, opposite contact or mating sides and related roughness. Mating sides "a" and "b" are interchangeable, as information about the actual related surface on specimen was missing from manufacture process. Roughness measurement was done with Mitutoyo surftest SJ-210. Measurement conditions obtained from manufacture are listed in Table 5. Exact details of the rest of the methods and machines used in manufacture process are missing.

Table 3: Roughness of 50 mm *in diameter specimens*

Specimen marking	Mating side	Ra [µm]	Specimen marking	Mating side	Ra [µm]
1	a	3,952	7	a	3,55
	b	3,267		b	3,135
2	a	3,198	8	a	3,155
	b	3,089		b	3,234
3	a	3,498	9	a	3,468
	b	3,472		b	3,239
4	a	3,283	10	a	3,434
	b	3,739		b	3,397
5	a	3,281	11	a	3,412
	b	4,113		b	3,24
6	a	3,217	12	a	3,397
	b	3,215		b	3,355

Table 4: Roughness of 25 mm *in diameter specimens*

Specimen marking	Mating side	Ra [µm]
13	a	3,531
	b	4,126
14	a	3,103
	b	3,094
15	a	3,274
	b	3,344

Table 5: Roughness measurement conditions from manufacture

Standard	JIS 1994	Number of sampling lenghts	4
Profile	Profile of roughness	λc[mm]	2,5
λs[µm]	8	Filter	Gauss

5.2 Specimen further preparations

After designing and manufacturing process, more modifications and preparations were done. The surface measurements, roughness modification, shielding and estimation of the mechanical properties.

5.2.1 Roughness modification

In order to measure and compare different roughnesses in experiments, three specimens were grinded on SINOWON GP-2 Grinder Polisher machine (Appendix, Figure 28). Specimens 1, 4 and 5 were chosen, because of the big roughness difference between their mating surfaces. Grinding was performed stepwise with five different grinding papers with ISO P grade. Beginning with 400, continuing 600, 1000, 2400 and finishing with 4000 grade. The machine is rotating with grinding paper and lubricates it with water. Specimen had to be held manually on rotating grinding paper. For manipulation with specimen, holder was designed and 3D-printed (Appendix, Figure 24 and 25). Grinded specimens are shown in Appendix, Figure 29, 30 and 31.

5.2.2 Roughness measurements

Specimens 1 and 7 were chosen for additional roughness measurements as samples. The reason was to confirm the roughness to be around Ra 3,2 µm and to obtain the rest of surface parameters if possible. Also surfaces of grinded specimens (1, 4 and 5) were measured Measurement was done with digital microscope KEYENCE VHX-6000 (Appendix, Figure 26 and 27). Parameters used for roughness evaluation are listed in Table 6, where λs, λc are profile filters. Parameters respect the ČSN EN ISO 4288 standards [7]. Measured surfaces were cleaned with technical alcohol before every measurement. The parameters Ra obtained from measurement are listed in Table 7

Table 6: Parameters used for roughness evaluation. [7]

Ra	Recommended magnification	λs [µm]	$\lambda c = Ir$ reference length [mm]	In=Ir×5 evaluation length [mm]
0,1<Ra≤ 2	×4000 − ×1000	2,5	0,8	4
2<Ra≤ 10	×1000 − ×500	8	2,5	12,5
10<Ra≤ 80	×500 − ×200	8	8	40

Table 7: Roughness parameters obtained from measurement.

Specimen marking	mating side	Ra [µm] from manufacture	Ra [µm] measured	Ra [µm] measured after grinding
1	a	3,952	2,85	0,24
	b	3,267	2,13	0,27
4	a	3,283	-	0,26
	b	3,739	-	0,24
5	a	3,281	-	0,25
	b	4,113	-	0,23
7	a	3,217	2,59	-
	b	3,215	3,1	-

The used machine could not evaluate the mean slope. Therefore raw data of profile were imported into Talymap gold software , which evaluated mean slope values. Also values for Ra were evaluated for comparison with the rest of known Ra. This was done only for specimen 1 as sample. Obtained values are listed in Table 8.

Table 8: Roughness parameters with slope for specimen 1, measured and evaluated.

Specimen marking	mating side	Ra [µm] from manufacture	Ra [µm] measured	Ra [µm] evaluated	m [rad] evaluated
1	a	3,952	2,85	2,85	0,164
	b	3,267	2,13	2,75	0,202

5.2.3 Waviness measurement

The same specimens as in Chapter 5.2.2 were measured for waviness as samples for the same profile. The reason is to confirm if the specimens have actually conforming rough surfaces. λc filter was used the same as in the roughness measurements (Chapter 5.2.2), λs was set equal to λc and λf profile parameter was set as the biggest possible. The values are listed in Table 9.

Table 9: Waviness measurements.

Specimen marking	mating side	w_a [µm] measured	w_a [µm] measured after grinding
1	a	1,04	0,76
	b	0,47	0,34
4	a	-	1,17
	b	-	1,14
5	a	-	0,87
	b	-	0,79
7	a	0,57	-
	b	0,72	-

All the specimens satisfy the limit for conforming rough surface. The limit is the average waviness w_a maximally four times the Ra roughness (Chapter 3.4.1). Only exception is grinded specimen 4. However the overlap is not that significant, therefore the surfaces of the specimen 4 are assumed also as conforming rough.

5.2.4 Shielding

In order to avoid heat leakage due to radiation through the lateral surface area of specimen or stack in test chamber, shielding was made. Shielding has to cover lateral area of specimen stack and copper plates with probes. Construction of copper plates with probes is described in [20]. Shielding has diameter of the component with biggest diameter, which are the copper plates with probes. Specimen stack is placed between these copper plates. Shielding have cut holes for wires from probes. Shielding itself has geometry of tube made from Upilex polyimide foam wrapped in Upilex polyimide foil. Both foam and foil, are highly heat resistant materials and avoid the avoid the heat leakage. Shielding has to be made separately for every stack with different amount of specimens. For measurements three shieldings were made. For one, three and six specimens in stack. Density of foam is 28,2194 $\mathrm{kg/m^3}$ and thickness is 10 mm. Thickness of foil is roughly 20 µm. The shielding is shown in Appendix, Figure 34.

5.2.5 Mechanical properties

In order to find out mechanical properties of material used for specimens (EN CW004A/ Cu-ETP), newer version of Czech version of the European Standard EN 13601:2002 was used [8]. According to standards, this material can have different mechanical properties depending on material condition. However the exact material condition of specimens stays unknown. Therefore only estimated properties, obtained from possible material conditions are used. This brings large error into calculations. Estimated values are in ranges between the maximum and minimum possible value. In Table 10 yield stress S_y, ultimate strength S_u (both in tensile) and Vickers microhardness are listed with minimum, maximum and average value.

Table 10: Specimens material mechanical properties [8].

S_y [MPa]			S_u [MPa]			HV [MPa]		
min.	max.	avg.	min.	max.	avg.	min.	max.	avg.
120	320	220	200	350	275	343,2	1128	735,5

Elastic modulus E and Poissson number μ also stay unknown and are not proposed in standards. Thus, estimated values of 130 GPa for elastic modulus and 0,33 for Poisson number are assumed. This values are generally used for elastic modulus and Poisson number of copper.

5.3 TCR evaluation method

Before the experimental measurements, the way how the resistances of the specimens and contacts looks like must be understood. This makes evaluation process of TCR possible. When two specimens are put between the HI and CI the circuit in Figure 10 is created. In such case the stack consists of two specimens. The TCR between the surfaces of HI, CI and specimens R_{SI}, the thermal resistance of specimens solid R_{SPEC} and the TCR between the specimen surfaces R_C are present in circuit. The resistances are in series.

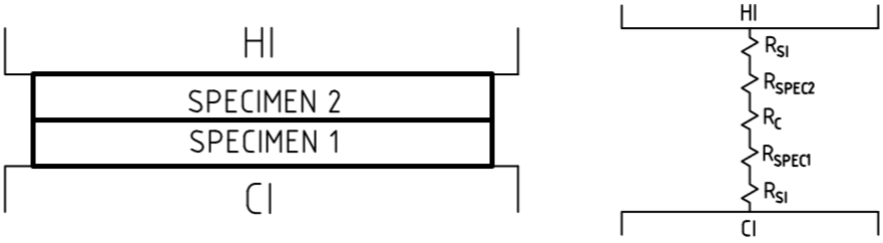

Figure 10: Two specimens in the stack, between the HI and CI.

Although, three TCRs are present, the TCRs between the specimen and interfaces (R_{SI}) cannot be used for adequate measurements. It is so, because many parameters of the interfaces are unknown or undefined. This would make theoretical calculations impossible. The TCR will be measured between the surfaces of the specimens (R_C), what requires at least two specimens in the circuit.

The total thermal resistance of the circuit is the sum of all the resistances in circuit, what can be written as:

$$R_{total} = R_C(n-1) + \sum_{i=1}^{n} R_{SPECi} + 2R_{SI} \tag{47}$$

where i is consecutive number of the specimen in stack and n is the number of specimens in stack. However eq.(47) is valid only, when both R_{SI} are considered to be equal and all the R_C are equal.

In order to obtain R_C, the rest of the resistances has to be known. R_{SPECi} can be calculated with eq.(3). R_{total} must be obtained from experimental measurement. R_{SI} can be obtained from experimental measurement with only one specimen in circuit, because then the R_{SI} is in direct dependency with R_{total}.

5.3.1 The contact multiplying effect

When two specimens are put into one stack (required minimum to measure R_C), the R_C is only one of the three TCRs in circuit and only one of the five resistances in total. In the results from experimental measurement the effect of R_C can occur only as very small

in comparison with the rest of the resistances. In order to make the effect of the TCR R_C more significant, the more specimens must be added into stack. It will make TCR R_C more significant in comparison with TCR R_{SI}. Of course by adding more specimens into stack, the effect of thermal resistance of specimen solids R_{SPEC} will also rise, but only proportionally with TCR R_C. Also the effect of R_{SPEC} is not that significant as the effect of TCR. The effect of adding more specimens into stack in order to make the TCR R_C more significant is the contact multiplying effect.

In order to have amount of the TCRs R_C at least equal to TCR R_{SI}, minimum of three specimens in stack should be used. The stack can be seen in Appendix, Figure 37 and 36. The exact amount of the specimens needed to make TCRs R_C significant enough is unknown and requires the experimental measurement.

6 Theoretical and experimental measurements

The basic measurement specification, the measurement plan and description of theoretical and experimental measurements are proposed.

6.1 Basic measurement specifications

The specifications of the experiment conditions are proposed and the premises for measurements are made.

6.1.1 Specification of experiment conditions

Actual experiment conditions can slightly differ from investigated ones (Chapter 3.4.7).

Obtained vacuum in test chamber was roughly 10^{-3} Pa. Contact pressures were obtained with weight of 9,12 kg, which yields load of 89,5 N. Pressure in contacts can slightly differ with weight of specimens themselves as they are put in stack. However, this is assumed as negligible in comparison to the rest of the weight. The nominal contact area of specimens with diameter of 50 mm, considering the hole and radiuses, is 1906,947 mm^2 and for specimens with diameter of 25 mm, it is 434,325 mm^2. Thus, nominal contact area (eq. (18)) results in 46916,5 Pa for larger and 205991,3 Pa for smaller specimens.

Temperature difference was measured from steady state heat transfer. The temperatures from HI and CI in test chamber were measured with probes in copper plates and data were recorded. CI temperature was held on temperature of $0 \pm 0,5$ °C. The reached heat load on HI was 4 W, what respects the interval in which MHS should be capable to operate (FPR5, Table 2.1).

6.1.2 Premises

1. For adequate measurement it is required that all the specimens in stack will have the same nominal roughness and diameter. The same roughness is needed for TCC evaluating method (Chapter 5.3). The same diameter will ensure that heat leakages due to radiation from mating surfaces will not occur.

2. The specimens in stack must be centered, what assure the Torlon dowels. Also drilled radiuses must be aligned to avoid mating surfaces being in no contact. This must be done manually with slight twist around the Torlon dowel. Therefore it is considered that all the specimens have their whole mating area in the contact.

3. Every measured stack has shielding avoiding heat leakages due to radiation through the lateral areas.

4. Actual created vacuum in experimental measurements is considered to be sufficient enough, to consider no heat leakages due the convection and the gap the TCC being equal to zero. Therefore, in every measurement (experimental or theoretical) is assumed that the heat is transferred only through the mating surfaces and only through the solid spots.

5. The eq.(47) must be valid. In case when TCRs actually differ, an average or estimated value must be used.

These premises are made, so the experimental and theoretical measurements can be later compared in Chapter 7.

6.2 Measurement plan

In order To carry out the experiments and compare the experimentally obtained values of the TCR with predicted ones, the measurement objectives are specified. The objectives are:

- To obtain the values of the TCR of contacts between the copper plates with probes and specimen (value of R_{SI}). It is needed for evaluation of R_C and has to be obtained for specimens with grinded surface as well as specimens with no roughness modification.
- To compare the TCR values evaluated from the experimental measurements with theoretical calculations.
- To compare the TCR values for specimens with different roughness and the specimens under different contact pressure.
- To find out how significant is the multiplying effect (Chapter 5.3.1). Therefore, to find out how many specimens is needed to put into stack, so the effect of TCR is significant enough to be relevant. Relevantly significant should be when the effect of TCR itself does not become negligible in comparison with the rest of resistances in circuit.
- To compare the effect of radiation heat leakage when specimens with different diameter are used. By other words, to find out, if the heat leakage due to radiation is negligible if the specimens with smaller diameter are used(in comparison with larger ones). If the radiation effect would be negligible, smaller diameter of specimens could be used in future measurements. This would save the material costs and potentially open the question of relevant diameter used for any specimens in test chamber.

In respect to measurement objectives the plan was made resulting into six measurements, that are listed with specifications in Table 11.

Table 11: Measurements overview.

Measurement marking	Specific specimens in stack/amount		Roughness obtained by	Diameter of stack [mm]	Avg. Ra roughness [µm]
No.1	6	/1	wire-cutting	50	3,2
No.2	1	/1	grinding	50	0,25
No.3	13; 14; 15	/3	wire-cutting	25	3,4
No.4	2; 6; 8	/3	wire-cutting	50	3,2
No.5	1; 4; 5	/3	grinding	50	0,25
No.6	2; 3; 6; 8; 10; 12	/6	wire-cutting	50	3,3

*Specimens are lined up from left to right as they were put into stack from below to upward.

Notes:

Specimen 6 was used in No.1. It was the most appropriate specimen because of it‘s both sides to be the similar roughness (Table 3). The similar roughnesses are optimal for the right evaluation of R_{SI} with eq.(47).

Specimen 1 was used in No.2. It was the most appropriate specimen because of it‘s both sides to be the similar roughness (Table 7). The similar roughnesses are optimal for the right evaluation of R_{SI} with eq.(47). However, in this case, probably any of the three grinded specimens could be used as all of them have similar roughness on both mating sides.

Specimens used in No.3 are: 13; 14; 15. The order is random as there are only these three specimens with smaller diameter.

Specimens used in No 4. are: 6; 2; 8. The reason for this order was to have 6 and 8 specimens in contact with interfaces as both have similar average roughness of their‘s mating sides (Table 3). Therefore values from No.1 could be used. Specimen 2 was used for it‘s roughness to be also around the similar values as 6 and 8.

Specimens used in No.5 are: 5; 4; 1. The order is random as all of the the grinded specimens have similar roughness (Table 7).

Specimens used in No.6 are: 6; 3; 12; 10; 2; 8. The reason for this order was to have 6 and 8 specimens in contact with interfaces as both have similar average roughness of their‘s mating sides (Table 3). Therefore values from No.1 could be used. The rest of specimens in stack are used because of their better roughness similarities to 6 and 8 in comparison with the rest of the specimens (7; 9; 11). Theirs order is random.

6.3 Experimental measurement

6.3.1 Test chamber

For experiments an experimental thermo-vacuum chamber at BUT is used. Test chamber can be seen in Figure 11. Vacuum, heat and regulation systems are connected to Test chamber. Thermo-resistors generate the heat at the HI. Then the heat transfers through the sample (or specimen) and copper plates with probes to the CI, that is connected to a tank by copper rod. To cool down the CI, the tank must be filled with liquid nitrogen. The CI temperature can be regulated by reheating to specific value. At different levels of thermal path in test chamber the temperature sensing probes are placed. The probes send the signals to a data store. Connection between the data store and probes in chamber is made by vacuum feed-through connector. The Mylar foil and Upilex foam insulate the thermally influenced copper components. [23] Further specification of test chamber are described in [20].

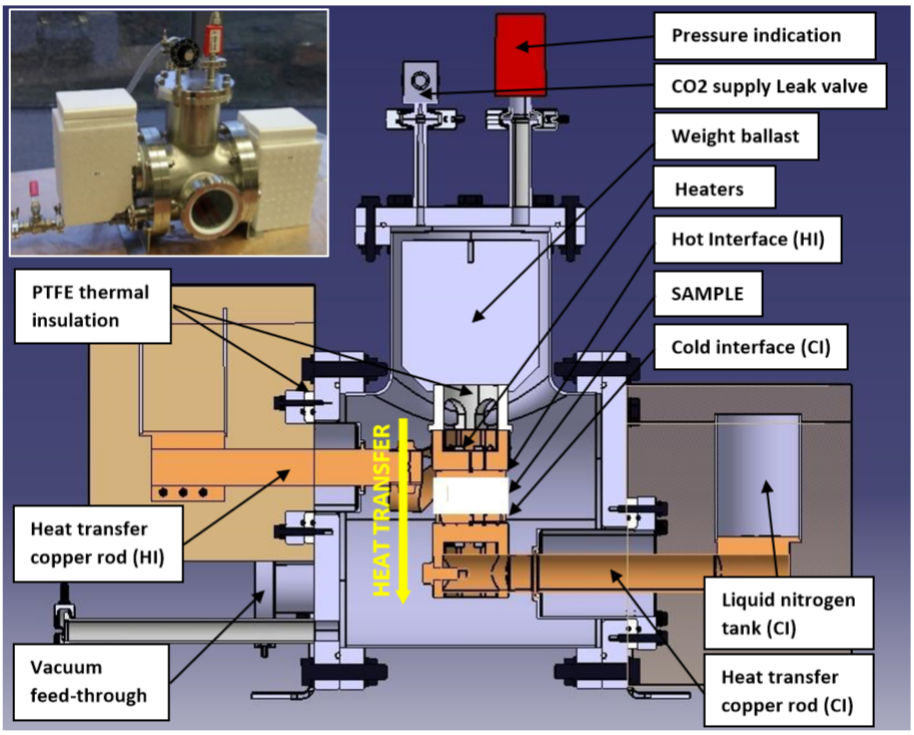

Figure 11: The thermo-vacuum test chamber. [23]

6.3.2 Test phase and evaluation of TCR

Stack, together with copper plates with probes and shielding are put between the components of test chamber simulating HI and CI. Before every installation all the specimens are cleaned with technical alcohol to avoid impurities in contacts. Test chamber and stack with shielding add into chamber can be seen in Appendix, Figure 32 and 33. The atmosphere is pumped out from test chamber and the cooling process of CI is initiated. Cooling is done manually with liquid nitrogen (periodically filled into tank) until the temperature of roughly 0 °C is reached. Then regulation of temperature on both HI and CI starts and continues until the steady state heat flow is obtained. Steady state is held at least 30 minutes to obtain adequate data from measurement. The data of temperatures are recorded during the whole measurement and stored for further evaluation of TCR.

Temperatures measured from probes are processed and the temperature difference ΔT is evaluated. The process of heat flow rate Q evaluation is described in [20]. When ΔT and Q are known, the thermal resistance R can be calculated by eq.(2) and eq.(3). Then the thermal resistance R can be substituted in eq.(47) as total thermal resistance R_{total}. This enables to calculate TCR R_C.

6.4 Theoretical measurement

To obtain theoretical values of TCR, following equations are used:

For σ_s eq.(11), for σ_1 and σ_2 eq.(12) and for σ_{Ra} (Ra) average values of roughness listed in Table 11 are used.

For m_s eq.(13), for m_1 and m_2 eq.(14) without multiplying σ by 10 is used.

For $m`_s$ eq.(15), for $m`_1$ and $m`_2$ eq.(16) are used.

For k_s eq.(17) is used, where k_1 and k_2 are equal to $390\,W/mK$.

For P eq.(18) is used, where $P = 46916,5\,\text{Pa}$ for larger specimens and $P = 205991,3\,\text{Pa}$ for smaller ones.

In order to select the TCC h_c equations from selected models (Table 2), firstly the type of deformation by Mikic was calculated using eq.(30). For H eq.(24), for $E`$ eq.(19) and mechanical properties from Chapter 5.2.5 were used. Maximum value of γ for specimens was found to be 0,12. It still less than 0,33, therefore the type of deformation is considered as predominantly plastic. Also the load is not assumed as large. Thus, eq. of correlations (27) and (29) will not be used. Also eq. of theoretical models (21) and (25) will not be used. These are too complex and correlations derived from them should be sufficient enough for comparison with experimental values in this work. Therefore, for every TCC model only one equation for h_c is used. The equations for every model are listed in Table 12.

For Hardness H eq.(24) is used in equations of CMY, Mikic, Yovanovich and Tien. For equations of Shlykov-Ganin and Malkov eq.(42) and for Mikic-Rohsenow Vickers microhardness are used. Mechanical properties used for hardness are listed in Table 10. All three, minimum, maximum and average values are used.

For R_{SPEC} eq.(47) is used.

Table 12: Models and used equations.

Model	Chapter	Equation	
CMY	4.3.1	$h_s = 1,45\frac{k_s m_s}{\sigma}\left(\frac{P}{H}\right)^{0,985}$	(23)
Mikic	4.3.2	$h_s = 1,13\frac{k_s m_s}{\sigma}(P/H)^{0,94}$	(28)
Yovanovich	4.3.3	$h_s = 1,25\frac{k_s m_s}{\sigma}\left(\frac{P}{H}\right)^{0,95}$	(31)
Tien	4.4.1	$h_s = 0,55\frac{k_s m`_s}{\sigma}\left(\frac{P}{H}\right)^{0,85}$	(40)
Shlykov-Ganin	4.4.2	$h_s = 2,1\times 10^4 k_s\left(\frac{P}{H}\right)$	(41)
Malkov	4.4.3	$h_s = 2,95\times 10^3 k\left(C\frac{P}{H}\right)^{0,66}$	(45)
Mikic-Rohsenow	4.4.4	$h_s = 0,9\frac{k_s m}{\sigma}\left(\frac{P}{H}\right)^{16/17}$	(46)

6.4.1 Measurement No.3 additional calculations

In measurement No 3. different diameter and contact pressure occurs. Also possible heat leakage due to radiation is assumed. Two situations are considered in this work. The first situation considers the heat leakage due to radiation as negligible and focuses on the comparison of different contact pressures between measurements No.3 and No.4. The second situation considers the heat leakage as not negligible and the aim is to find the amount of heat that is transferred due to radiation in comparison with heat transferred due to conduction.

In both situations is needed to evaluate the TCR R_{SI} for smaller specimens in mea-

surement No.3[2]. Then, in the first situation the TCR R_C when radiation is negligible can be obtained. In the second situation to evaluate the TCR R_C is also needed, however TCR R_C obtained from the first situation cannot be used.

For the evaluation only the semi-experimental solution is used. Assuming that average roughness difference between the specimens in the measurement No.1, No.3 and No.4 is negligible (only 0,1 and 0,2 µm) the R_{SI} value is evaluated from experimentally measured value in measurement No.1. Similarly the value of R_C in the second situation is evaluated from measurement No.4.

The aim of the evaluation process is to obtain the values for the measurement No.3 that takes the different area and contact pressure into account.

Therefore TCR value must be converted to K, divided by area of specimen used in No.1 or No.4 and than multiplied by area of the smaller specimens in No.3. This will take the different area into account but, still the contact pressure difference must be considered.

How much exactly the contact pressure influence the TCR is unknown. Using the TCC models equations (Table 12) it can be seen that TCC h_s is proportional to pressure with exponent, where exponent varies in different equations. The range in which exponent varies is from 0,66 to 1. Thus, the contact pressure quotient of different contact pressures in measurements can be powered by exponent in this range and the TCC can be multiplied by obtained value. It will further results into TCR values range applicable for measurement No.3. The process can be expressed by relationship:

$$R_{No.3} = \frac{A_{No} R_{No}}{A_{No.3}} \left(\frac{P_{No}}{P_{No.3}} \right)^z \tag{48}$$

$$z = 0,66; 1$$

Variables with index $No.3$ are those in measurement No.3, those with No index are from measurement No.4 or No.1. Exponent z is the pressure contact exponent.

This method can show as strongly inaccurate but can be used for rough results comparison in order to create a picture of the contact pressure or radiation effect. When R_{SI} is obtained for the first situation the eq.(47) is used for TCR R_C value range evaluation. The range is further used for comparison with predictions of models.

In the second situation evaluated R_{SI} and R_C value ranges are substituted into eq.(47). This results to values of R_{total}, that are used for evaluation of $Q_{conduction}$ by eq.(10). The values of R_{SI} and R_C substituted in eq.(47) must be the values obtained by the same contact pressure exponent. Finally, by eq.(4) the minimum and maximum values for $Q_{radiation}$ are obtained, where Q_{total} is the value obtained from experimental measurement No.3 and $Q_{convection} = 0$.

To find out if the values obtained by semi-experimental method are relevant and physically possible, the $Q_{radiation}$ assuming the range of possible emissivities ε [−] is calculated and compared. The copper plates (HI and CI) have the diameter of 56 mm. The area

[2]Ideally the TCR R_{SI} should be obtained by experimental measurement. However, in this work the experimental measurement of R_{SI} for purposes of No.3 measurement will not be made.

of copper plates in no contact in measurement No.3 makes 2028,68 mm^2. Emissivity of copper plates is estimated to be in the range from 0,04 to 0,8. These are the limits of common values for the copper surfaces. The heat transferred due to radiation is calculated with relationship:

$$Q_{radiation} = \frac{A \times \sigma_B \times \varepsilon \times (T_1^4 - T_2^4)}{(2 - \varepsilon)} \tag{49}$$

where T_1 and T_2 are the temperatures on the HI and CI substituted in Kelvins $[K]$, σ_B is Stefan-Boltzmann's constant ($\sigma_B = 5,669 \times 10^{-8}\, W/mK$) and A is an area of the radiation exchange. The eq.(49)applies for two parallel surfaces when all the radiated heat from one surface strikes the other one.

7 Results and comparison

The experimental measurements were carried out. The results are proposed and comparison between the measurements is made. The obtained input data from experimental measurements are ΔT (where CI temperature is 0 °C) and evaluated Q_{total}, K_{total} and R_{total}. The data are listed in Table 13.

Table 13: The data obtained from experimental measurement.

Meas.	ΔT [°C]	Q_{total} [W]	K_{total} [W/K]	R_{total} [K/W]
No.1	8,49	4,08	0,48	2,083
No.2	8,64	4,53	0,524	1,908
No.3	22,22	3,59	0,161	6,211
No.4	21,15	4,15	0,196	5,102
No.5	37,34	3,64	0,098	10,204
No.6	36,71	3,89	0,106	9,434

At first glance, the result shows that total resistance decreased with smoother surface when measurements No.1 and No.2 are compared. It agrees with theory. However the total resistance increased with the smoother surface when measurements No.4 and No.5 are compared. It disagrees with theory. Comparing measurement No.3 and No.4 the resistance increased with higher contact pressure, although TCR is inversely proportional to the TCC that increases with the higher contact pressure. Comparing measurements No.1, No.4, No.6 the total resistance increases. This agrees with theory.

7.1 Thermal resistance of specimens

Thermal resistances of specimens solid R_{SPEC} for specimens with different diameter are listed in Table 14. These values applies for all the specimens used in measurements and are used for the TCR evaluation method (Chapter 5.3).

Table 14: Thermal resistance of specimens.

Diameter [mm]	50	25
R_{SPEC} [K/W]	0, 00672	0, 02952

The estimated thermal conductivity was $k = 390$ W/mK. In order to compare the effect of thermal conductivity of the material k on R_{SPEC}, the values similar to the estimated one were added and the resulting R_{SPEC} is compared. The values of thermal conductivity are chosen approximately in the range of pure coppers. The values are listed in Table 15.

Table 15: The effect of thermal conductivity on thermal resistance of specimen R_{SPEC}.

k [W/mK]	R_{SPEC} [K/W]		Difference
	Dia. 50 mm	Dia. 25 mm	
400	0,00655	0,02878	-2,50 %
390	0,00672	0,02952	0,00 %
380	0,00690	0,03030	2,63 %
350	0,00749	0,03289	11,43 %

Results show 11,43 % increase of specimen thermal resistance when thermal conductivity decreased on 350 W/mK. But still, the resistance is small and the increase makes only $7,7 \times 10^{-4}$ K/W.

7.2 TCR between the interface and specimen surfaces

Thermal resistances R_{total} from experimental measurements No.1 and No.2 , with one specimen in stack and different roughnesses are obtained. Derived values of thermal resistances R_{SI} are obtained. The resistances are listed in Table 16.

Table 16: Total resistances and TCRs from measurements No.1 and No.2

Measurement	No.1	No.2
R_{total} [K/W]	2,083	1,908
R_{SI} [K/W]	1,026	0,951

The results shows that thermal resistances of specimen with higher average roughness (Ra $3,2\,\mu m$) in measurement No.1 is higher than the thermal resistance of the grinded specimen with lower average roughness (Ra $0,25\,\mu m$) in measurement No.2. This is in agreement with the theory. However, the difference is not so significant. Remarkable is the fact that TCR R_{total} is approximately in agreement with results obtained in previous study [20]. Obtained values are further used for TCR evaluation method (Chapter 5.3).

Additionally R_{SI} for smaller specimens (diameter of 25 mm) used in measurement No.3 was semi-experimentally evaluated for minimum and maximum value on the basis of measurement No.1. The values are listed in Table 17.

Table 17: Semi-experimental TCR range for measurement No.3

R_{SI} [K/W] meas. No.3	
min.	max.
1,026	1,7

The semi-experimental results show that higher pressure caused by reduced area (with constant load) can only increase TCR or do not change it at all. It results from models assuming different contact pressure exponent. With exponent $z = 1$ TCR does not change.

7.3 Results and comparison of theoretical and experimental measurements

Theoretical and experimental results for TCR R_C from measurements No.3, No.4, No.5 and No.6 and the values of R_{total} obtained from experimental measurements are listed in Table 18. The experimental TCR R_C in measurement No.3 have listed semi-experimental minimum and maximum values evaluated on basis of measurement No.1 assuming heat leakage as negligible. All the models have listed minimum and maximum values in respect to range of values for mechanical properties(Chapter 5.2.5) and the average value TCR R_C.

Table 18: TCRs obtained from theoretical and experimental measurements for measurements No.3, No.4, No.5 and No.6

Meas.	Theoretical values of TCR Rc [K/W]																					Experimental values of TCR [K/W]	
	CMY			Mikic			Yovanovich			Tien			Shlykov-Ganin			Malkov			Mikic-Rohsenow				
	min.	max.	avg.	min.	max.	avg.	min.	max.	avg.	min.	max.	avg.	min.	max.	avg.	min.	max.	avg.	min.	max.	avg.	Rc	Rtotal
No.3	0,1209	0,3176	0,2193	0,1108	0,2787	0,1948	0,1079	0,2742	0,1911	0,0927	0,2134	0,1530	0,8188	1,4330	1,1259	0,2296	0,3321	0,2808	0,1898	0,5818	0,3858	1,36/2,04	6,2111
No.4	0,1140	0,2996	0,2068	0,0978	0,2459	0,1719	0,0967	0,2455	0,1711	0,0716	0,1648	0,1182	0,8188	1,4330	1,1259	0,1333	0,1929	0,1631	0,1678	0,5143	0,3411	1,5149	5,1020
No.5	0,0248	0,0652	0,0450	0,0213	0,0535	0,0374	0,0210	0,0534	0,0372	0,0155	0,0358	0,0257	0,8188	1,4330	1,1259	0,0247	0,0358	0,0303	0,0365	0,1119	0,0742	4,1409	10,2041
No.6	0,1161	0,3052	0,2106	0,0996	0,2505	0,1751	0,0985	0,2501	0,1743	0,0729	0,1679	0,1204	0,8188	1,4330	1,1259	0,1361	0,1969	0,1665	0,1709	0,5239	0,3474	1,4683	9,4339

7.3.1 Measurement No.3 comparison

In Figure 12 results from measurement No.3 are shown. Only model able to predict TCR is Shlykov-Ganin model in the range of higher values of mechanical properties. This model is strongly out standing with average value only 1,2 times lower that the lower limit of the semi-experimentally measured TCR . The rest of the models predicts the TCR on average 6,26 times lower than is the semi-experimentally measured TCR when the lower limit and average values of models are taken into account. Assuming the average values of models, the lowest values predicted Tien model, that are 8,88 times lower. Except the Shlykov-Ganin model, the biggest values predicted Mikic-Rohsenow model, that are 3,52 times lower. In Figure 13 predictions in lower axis scale of TCR are shown.

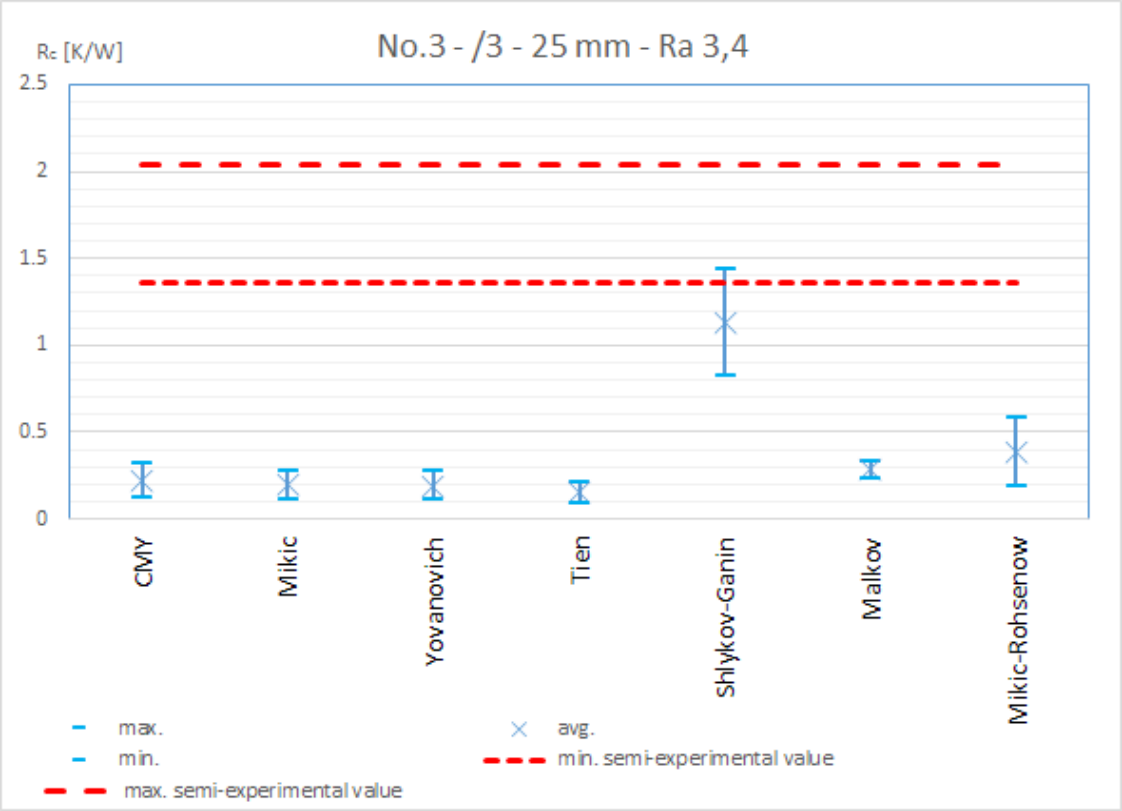

Figure 12: The results of the measurement No.3.

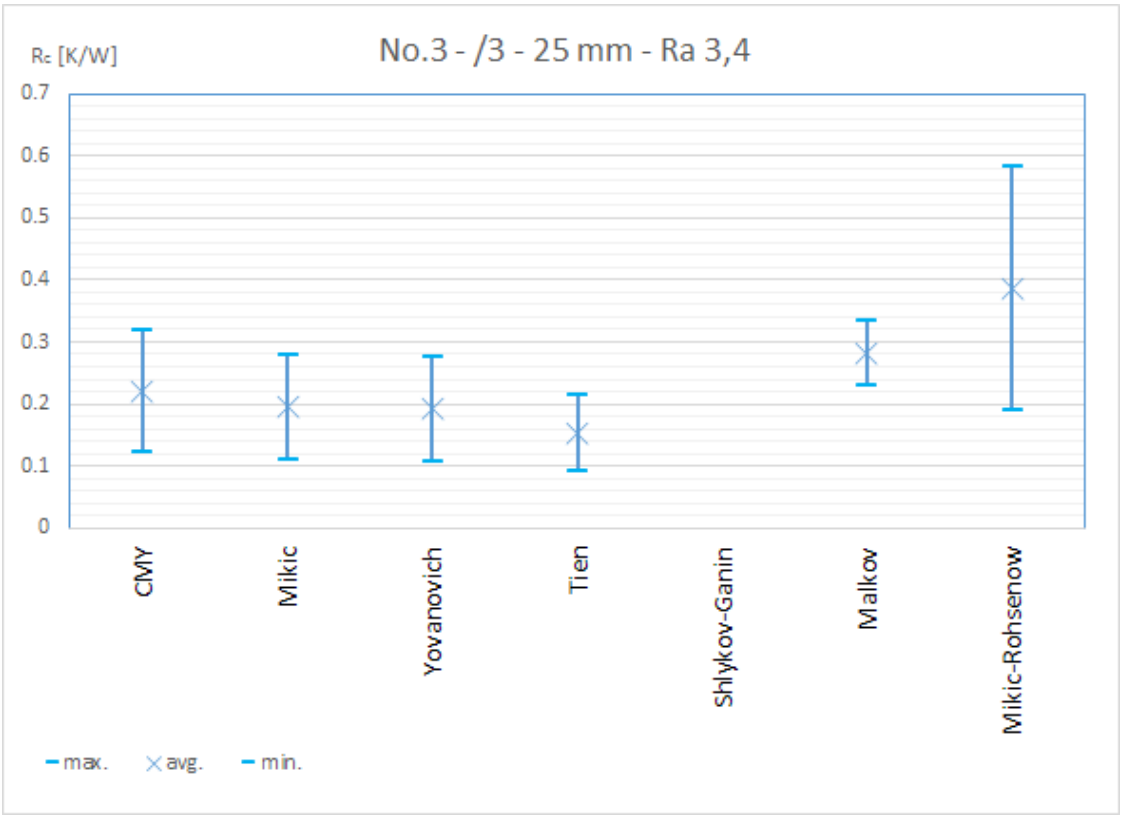

Figure 13: The results of the measurement No.3 in lower axis scale.

7.3.2 Measurement No.4 comparison

In Figure 14 results from measurement No.4 are shown. Not even one model is able to predict the experimentally measured TCR. Shlykov-ganin model is closest to the experimentally measured value with average value, that is only 1,35 times lower. The rest of the models predicts the TCR on average 8,59 times lower than is the experimentally measured TCR when average values of models are taken into account. Assuming the average values of models, the lowest values predicted Tien model, that are 12,81 times lower. Except the Shlykov-Ganin model, the biggest values predicted Mikic-Rohsenow model, that are 4,44 times lower.

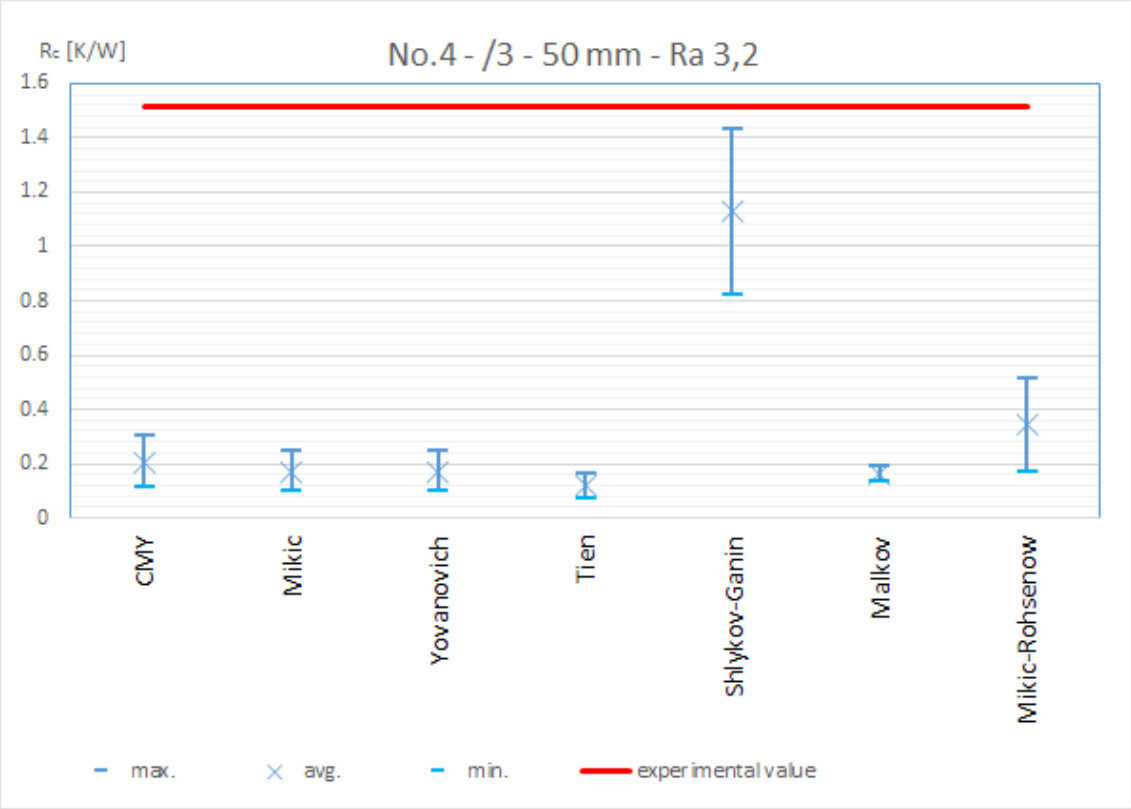

Figure 14: The results of the measurement No.4.

7.3.3 Measurement No.5 comparison

In Figure 15 results from measurement No.5 are shown. Not even one model is able to predict the experimentally measured TCR. Shlykov-ganin model is closest to the experimentally measured value with average value, that is only 3,68 times lower. The rest of the models predicts the TCR on average 111,14 times lower than is the experimentally measured TCR when average values of models are taken into account. Assuming the average values of models, the lowest values predicted Tien model, that are 160,84 times lower. Except the Shlykov-Ganin model, the biggest values predicted Mikic-Rohsenow model, that are 55,76 times lower. In Figure 16 predictions in lower axis scale of TCR are shown.

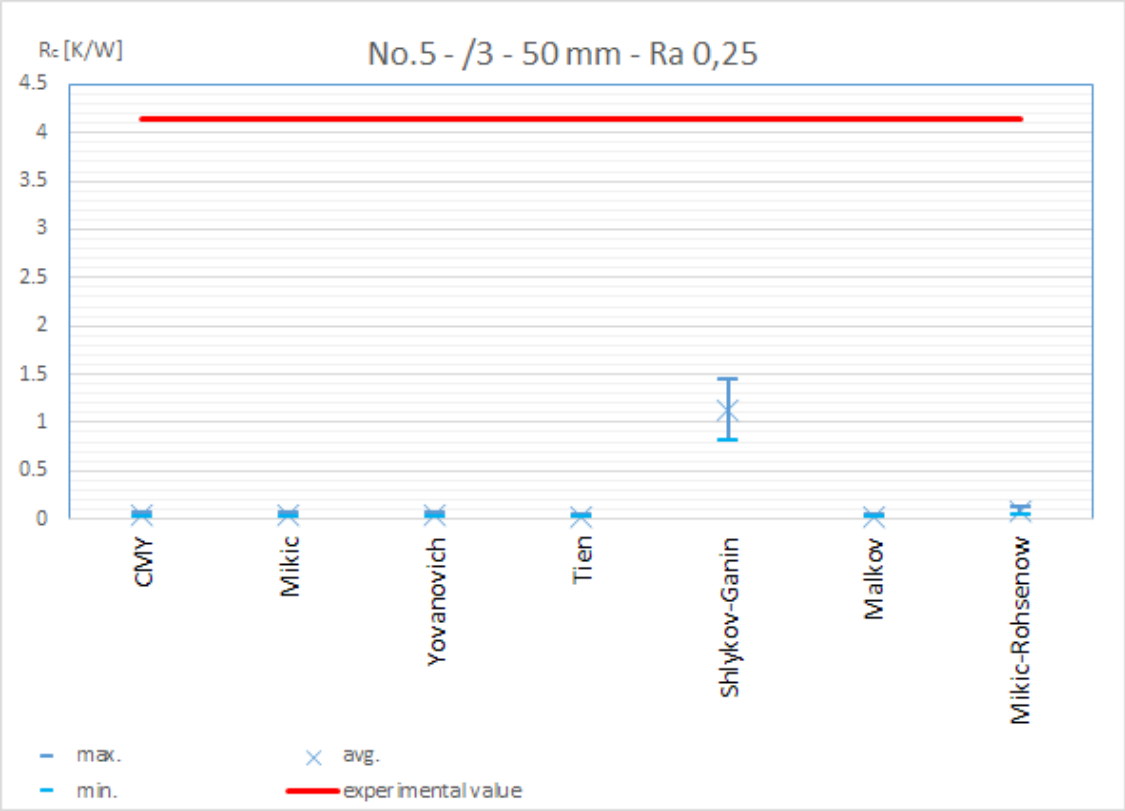

Figure 15: The results of the measurement No.5.

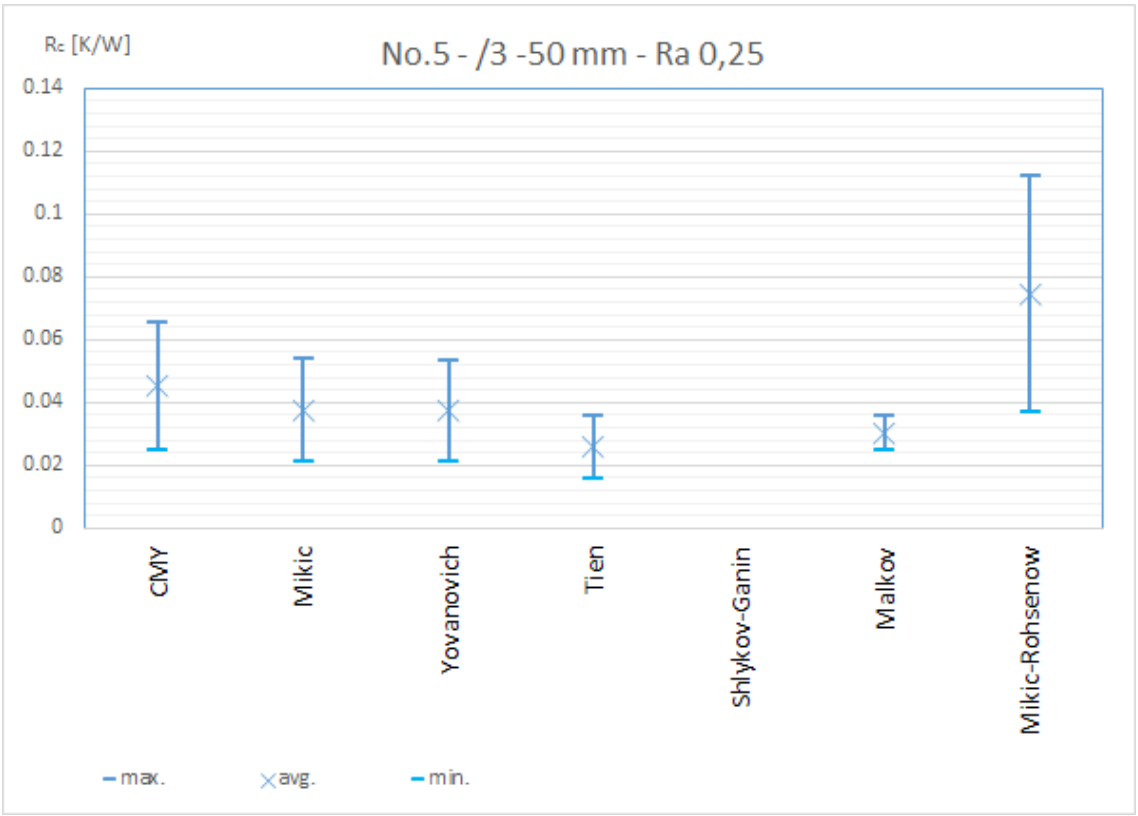

Figure 16: The results of the measurement No.5 in lower axis scale.

7.3.4 Measurement No.6 comparison

In Figure 17 results from measurement No.6 are shown. Not even one model is able to predict the experimentally measured TCR. Shlykov-ganin model is closest to the experimentally measured value with average value, that is only 1,3 times lower. The rest of the models predicts the TCR on average 8,16 times lower than is the experimentally measured TCR when average values of models are taken into account. Assuming the average values of models, the lowest values predicted Tien model, that are 12,19 times lower. Except the Shlykov-Ganin model, the biggest values predicted Mikic-Rohsenow model, that are 4,23 times lower.

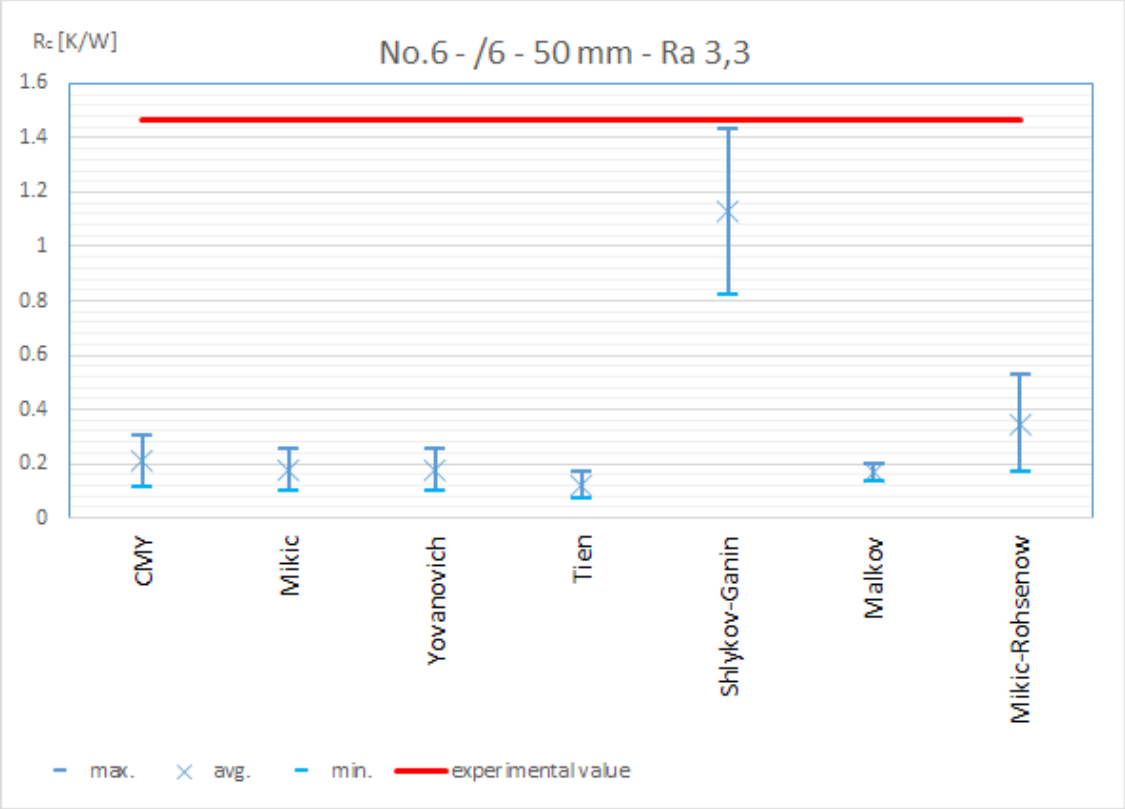

Figure 17: The results of the measurement No.6.

7.3.5 Overall comparison

In measurements not even one model predicted the semi-experimentally or experimentally measured values of TCR except the Shlykov-Ganin model in measurement No.3. However this model is strongly outstanding in all the measurements and actually predicts the same TCR all the time as can be seen in Table 18. The one reason is that the model is insensible to the change of the contact pressure by the change of the area (constant load) and the second is that model does not take the surface roughness in consideration at all. Thus, the Shlykov-Ganin model right prediction of TCR in measurement No.3 is probably only the coincidence. From the rest of the models always Tien model predicted the lowest values and Mikic-Rohsenow the biggest values. The possible reason why the models disagreed with predictions is the experimental contact pressure, contact temperature and the other factors to be out of the range the models were verified for. Another reason it that models use mostly the correlated values of many parameters, that can be measured instead of estimation and evaluation.

7.4 Radiation heat leakage comparison

Amount of radiation heat leakage is obtained in situation when radiation is assumed as not negligible in measurement No.3. In measurement No.3 the three specimens with diameter of 25 mm and average Ra roughness of 3,4 µm were used. Two methods (or solutions) of evaluating the heat leakage due to radiation or the heat transferred due to radiation across the surfaces of copper plates in no contact are used and compared. Both methods are described in Chapter 6.4.1.

For the semi-experimental method the minimum and maximum values are listed in Table 19.

Table 19: Radiation share evaluated by semi-experimental method.

Q_{total}=3,59 W		
z	$Q_{radiation}$ [W]	Radiation share
0,66	1,572	43,79%
1	0,266	7,41%

This method evaluated the values from the values experimentally measured in the measurement No.4. The basic principle was to use the semi-experimentally evaluated TCR values to calculate $Q_{conduction}$ and substitute it with experimentally measured Q_{total} to obtain $Q_{radiation}$. The results show that the heat transferred due to radiation is at least $7,417\%$ for contact pressure exponent equal to 1 and at most 43.786% for contact pressure exponent equal to 0,66.

For the method considering emissivity in the range from 0,04 to 0,8 the minimum and maximum values are listed in Table 20.

Table 20: Radiation share calculated theoretically.

Q_{total}=3,59 W		
ε	$Q_{radiation}$ [W]	Radiation share
0,04	$4,799 \times 10^{-3}$	0,13%
0,8	0,1567	4,37%

This method is theoretical and directly calculates the $Q_{radiation}$. The results show that the heat transferred due to radiation is at least $0,13\%$ for emissivity equal to 0,04 and at most $4,37\%$ for emissivity equal to 0,8.

The first method has probably large errors as the used values are only semi-experimentally evaluated and the used method is actually not verified. Also assumes the possible effect of the contact pressure exponent z. The second, theoretical method also uses only the estimated values of emissivity ε. On the other hand, this method is direct and origins from the heat transfer theory in which is generally used. Also the method was used already in MHS project [23]. Therefore, it is assumed that this method will give more relevant results than the semi-experimental one and the heat transferred due to radiation is actually low in comparison with the heat transferred due to conduction. Nevertheless,

this comparison is only indicative and only shows the approximate values of the radiation share in the measurements.

7.5 Contact pressure differences comparison

The contact pressure difference between measurements No.3 and No.4, in case when radiation is considered as negligible in No.3 is compared. In measurement No.3 the three specimens with diameter of 25 mm and average Ra roughness of 3,4 µm were used. In measurement No.4 the three specimens with diameter of 50 mm and average Ra roughness of 3,2 µm were used. Average roughness difference is only 0.2 µm, therefore is neglected. The pressure in contact has increased 4,39 times in measurement No.3 with constant load. The experimental values of R_C in measurement No.3 are evaluated by semi-experimental method (Chapter 6.4.1).

Table 21 shows the results with quotient q of average values, that only says how many times the TCR increased with higher pressure caused by reduced area in measurement No.3.

Table 21: TCRs obtained from theoretical and experimental measurements for measurements No.3 and No.4 with quotient.

Meas.	Theoretical values of TCR R_C [K/W]																				Experimental values of TCR [K/W]	
	CMY			Mikic			Yovanovich			Tien			Shlykov-Ganin			Malkov			Mikic-Rohsenow				
	min.	max.	avg.	min.	max.	avg.	min.	max.	avg.	min.	max.	avg.	min.	max.	avg.	min.	max.	avg.	min.	max.	avg.	R_C	R_{total}
No.3	0,1209	0,3176	0,2193	0,1108	0,2787	0,1948	0,1079	0,2742	0,1911	0,0927	0,2134	0,1530	0,8188	1,4330	1,1259	0,2296	0,3321	0,2808	0,1898	0,5818	0,3858	1,36/2,04	6,2111
No.4	0,1140	0,2996	0,2068	0,0978	0,2459	0,1719	0,0967	0,2455	0,1711	0,0716	0,1648	0,1182	0,8188	1,4330	1,1259	0,1333	0,1929	0,1631	0,1678	0,5143	0,3411	1,5149	5,1020
q			1,0602			1,1332			1,117			1,2946			1			1,7212			1,1312	0,9/1,35	1,2174

The most sensible theoretical model for contact pressure is Malkov model, that assumes contact pressure exponent 0,66. On the other side, the less sensible is the Shykov-Ganin, which considers contact pressure exponent 1. The fact that contact pressure difference is caused by the reduced area and not by the load is important, because the most of the influence of the area is eliminated when TCC values are converted to TCR values and then the contact pressure exponent is the only influencing parameter. While the contact pressure has increased 4,39 times, the models predicts the increase to be 1,2 times when average of averages is taken into account. This agrees with the range of values for semi-experimental R_C. Also it is in agreement with experimental results of R_{total} that increased 1,217 times. The R_{total} includes also the resistances of specimens, however they are too a small and the most of the circuit is created by TCRs that are uniformly influenced by the change of the contact pressure. Such results indicates, that radiation heat leakage is probably negligible and that the measurements were successful.

7.6 Number of specimens in stack comparison

The effect of the number of specimens in stack is compared between measurement No.4 with three specimens in stack and No.6 with six specimens in stack. The average roughness difference is only 0.1 µm and all the specimens have the same diameter of 50 mm. The average roughness difference is neglected. Table 22 shows the results with quotient q of average values, that only says how many times the TCR increased with higher amount of specimens in stack in measurement No.6.

Table 22: TCRs obtained from theoretical and experimental measurements for measurements No.4 and No.6 with quotient.

Meas.	Theoretical values of TCR R_C [K/W]																				Experimental values of TCR [K/W]	
	CMY			Mikic			Yovanovich			Tien			Shlykov-Ganin			Malkov			Mikic-Rohsenow				
	min.	max.	avg.	min.	max.	avg.	min.	max.	avg.	min.	max.	avg.	min.	max.	avg.	min.	max.	avg.	min.	max.	avg.	R_C	R_{total}
No.4	0,1140	0,2996	0,2068	0,0978	0,2459	0,1719	0,0967	0,2455	0,1711	0,0716	0,1648	0,1182	0,8188	1,4330	1,1259	0,1333	0,1929	0,1631	0,1678	0,5143	0,3411	1,5149	5,1020
No.6	0,1161	0,3052	0,2106	0,0996	0,2505	0,1751	0,0985	0,2501	0,1743	0,0729	0,1679	0,1204	0,8188	1,4330	1,1259	0,1361	0,1969	0,1665	0,1709	0,5239	0,3474	1,4683	9,4339
q			1,0186			1,0186			1,0186			1,0186			1			1,0205			1,0186	0,9692	1,849

The results shows no significant increase for predictions in measurement No.6 and only small decrease for experimental results R_C. Also it can be seen in Figures 17 and 14 in Chapter 7.3.2, that the results are similar. The predictions in measurement No.4 are 8,59 lower and in measurement No.6 8,16 times lower than experimental results. The experimental results agrees with theory as the TCRs should be the same. This indicates that experimental measurements are successful.

From the results it can be seen how significant is the effect of TCR R_C in the circuit. The percentage share o types of thermal resistances in circuit are listed in Table 23.

Table 23: Percentage share of thermal resistances in circuit.

Meas.	Percentage share		
	Rc	Rsi	Rspec
No.4	59,38%	40,22%	0,4%
No.6	77,82%	21,75%	0,43%

For six specimens with average Ra roughness of 3,3 µm the share of TCR R_C in the circuit is up to 77,82%. However, three specimens in stack with average Ra roughness of 3,2 µm are sufficient enough to still have the major share.

7.7 Roughness differences comparison

The effect of the surface roughness of specimens is compared between measurement No.4 and No.5. In both measurements three specimens are used, with the same diameter of

Table 24: TCRs obtained from theoretical and experimental measurements for measurements No.4 and No.5 with quotient.

Meas.	Theoretical values of TCR R_C [K/W]																				Experimental values of TCR [K/W]	
	CMY			Mikic			Yovanovich			Tien			Shlykov-Ganin			Malkov			Mikic-Rohsenow				
	min.	max.	avg.	min.	max.	avg.	min.	max.	avg.	min.	max.	avg.	min.	max.	avg.	min.	max.	avg.	min.	max.	avg.	R_C	R_{total}
No.4	0,1140	0,2996	0,2068	0,0978	0,2459	0,1719	0,0967	0,2455	0,1711	0,0716	0,1648	0,1182	0,8188	1,4330	1,1259	0,1333	0,1929	0,1631	0,1678	0,5143	0,3411	1,5149	5,1020
No.5	0,0248	0,0652	0,0450	0,0213	0,0535	0,0374	0,0210	0,0534	0,0372	0,0155	0,0358	0,0257	0,8188	1,4330	1,1259	0,0247	0,0358	0,0303	0,0365	0,1119	0,0742	4,1409	10,2041
q			0,2177			0,2177			0,2177			0,2177			1			0,1859			0,2177	2,7334	2

The theoretical results show that TCR increases with higher roughness in measurement No.4 and decreases 4,708 times with smoother surfaces in measurement No.5. However, the experimental results are in strong disagreement with theory. Experimentally measured values show the increase of the TCR R_C to be 2,733 times higher with smoother surface. The measurement No.5. shows significant error and the obtained values are not relevant for comparison. It is assumed that significant out-of flatness found on specimen 5 used in measurement No.5 after grinding could lead to deficient contact of mating sides. This would explain the high values of TCR.

8 Discussion and recommendations

The results from the experimental and theoretical measurements were carried out, compared and will be discussed in this Chapter. On the basis of the work and results, the recommendations for further work are proposed. The results showed that:

Not even one model (used in this work) predicts the TCR correctly. Thus any mathematical model for predictions was found. The one exception occurred in the measurement No.3, when Shlykov-Ganin model predicted the TCR. However it is assumed to be only a coincidence.

The contact pressure increase caused by the area decrease actually enlarge the TCR. The exact dependence of TCR on the contact pressure stays unknown.

The measurement No.5 is considered as unsuccessful. The results significantly disagreed with the theory. It was later found, that one specimen in the measurement has poor flatness, that probably lead to a deficient contact. Thus, the results are assumed as not relevant.

The radiation heat leakage, when specimens with the half of a diameter are used is roughly 0,1% to 5%. However using the semi-experimental method it seems to be roughly 7% to 44%. The results evaluated by semi-experimental method are not preferred as they include a large error and the correctness of the method is not verified. In the case when radiation would be only 5% or less, it could be assumed as negligible.

It does not make any significant difference, if three or six specimens with average Ra roughness roughly $3,2\,\mu m$ are used in the stack. Thus, the stack with only three specimens can be used. This will decrease the roughness dispersion and enable to modify more specimen surfaces as there will be no need to have six specimens with the same roughness. When three specimens were used, the TCRs still had over the half of the share in circuit total resistance. However, this does not have to apply for three specimens with different average roughness as the share should decrease with smoother surfaces.

The thermal resistance of the specimens is small, even when the assumed thermal conductivity differed in tens. In the circuit, it has a minimum effect. The TCRs have the biggest influence on the thermal path.

The surface parameter measurement can significantly vary according to standards and the used machine or software. This brings uncertainties into measurements.

The specimens can be assumed as conforming rough according to results from waviness measurement

For the further work it is recommended:

To measure the actual surface parameters (including the specimens and interfaces) with different machines and softwares and compare the results. Besides the roughness parameters, also the waviness and the geometry parameters for all the specimens should be obtained. This would show if all the specimens are conforming

rough and the error from surface correlations will be eliminated. The effect of different surface measurements should be considered.

To measure the rest of the parameters influencing the TCR. The actual thermal conductivity of copper (EN CW004A/ Cu-ETP). This will eliminate the error of estimated value. The emissivity of specimens, to reduce the range and eliminate the error. The actual mechanical properties of specimens. Also the microhardness dependency. This would reduce the range and eliminate the error.

To make additional adjustments. Upgrade the shielding with the Mylar foil and more layers. Fix the specimen with poor flatness used in the measurement No.5 or consider preparation of a new one. Uniform the roughness of the specimens, by surface modification to have actually the specimens with the same roughness in one stack.

To make considerations about the future measurements. Consider possible errors of measured temperatures. Consider different methods od surface modification. Consider the use of the interstitial materials as graphite foils, powders and thermal greases in order to enhance the TCC, and reduce the TCR. Consider the use of the different materials for the specimens as aluminium or different types of copper. Consider the use of the different heat load on HI. Consider the different CI temperatures for measurements. Repeat the measurement No.5 with appropriate specimens. Measure the TCR for one smaller specimen in stack to eliminate the error in measurement No.3. Examine the actual radiation heat leakage when smaller specimens are used. Initiate the more extensive measurements with different specimen roughness in contacts. Carry out the measurements with different loads, to obtain different contact pressures.

Prepare the next measurements based on the results, assumptions and recommendations in this work and continue in the finding of the suitable mathematical model for TCR prediction.

9 Conclusion

In 2015, the Institute of Aerospace Engineering, University of Technology in Brno was commissioned by Arescosmo to test the BBs of miniaturised heat switch developed for European Space Agency. The developed BBs of MHS were found to be dysfunctional, mainly because of the poor contacts in construction causing the high TCR and low conductance. The preparations of third BB has begun and one of the aims became to optimize the TCR in order to deal with a low conductance. It initiated this work that takes the first step in optimization of the TCR in the MHS. To describe TCR and find the suitable model for its prediction by comparison of experimental and theoretical measurements. For experiments, the vacuum test chamber is used.

Thus, TCR is defined and the factors the TCR depends on are described. The main factors the TCR depends on are: the surface parameters, the thermal conductivity, the contact pressure, the hardness and interstitial gap. The investigated conditions, for which the models are tested are proposed. The conditions are chosen in respect to MHS requirements.

The TCR (TCC) models are reviewed, selected and described. The seven models are selected and described with the parameters and correlations they use.

For experimental comparison with models, the copper specimens with different roughness and diameters are designed and manufactured. Additional surface measurements and modification by grinding for some specimens are made and mechanical properties are estimated. The measurements showed the specimens differ in roughness and the measured roughness can strongly differ with standards and machines used for the measurement. Waviness measurements showed the specimens surfaces to be conforming rough.

Six experimental and theoretical measurements of the TCR were specified, planned and carried out. Besides, the main objective of finding the suitable mathematical model for prediction, the additional objectives are proposed. Results showed that not even one model was found to agree with experimental results, except the Shlykov-Ganin model in measurement No.3. However it is assumed to be only a coincidence. All the measurement results were compared and discussed. On the basis of work and results the recommendations for further work were proposed.

10 Bibliography

[1] ANTONETTI, V. W., T. D. WHITTLE and R. E. SIMONS. An Approximate Thermal Contact Conductance Correlation. *Journal of Electronic Packaging* [cit. 2019-05-03]. 1993, **115**(1), 131. ISSN 10437398. Available: doi:10.1115/1.2909293

[2] ANTONETTI, V.W. and M.M. YOVANOVICH. Using Metallic Coatings to Enhance Thermal Contact Conductance of Electronic Packages. *Journal of Heat Transfer Engineering* [online] [cit. 2019-05-11]. 1988, **9**(3), 85-92. ISSN 0145-7632. Available: doi:10.1080/01457638808939674

[3] ASIF, Mohammad and Andallib TARIQ. Correlations of Thermal Contact Conductance for Nominally Flat Metallic Contact in Vacuum. *Experimental Heat Transfer* [online][cit. 2019-04-13]. 2016, **29**(4), 456–484. ISSN 0891-6152. Available: doi:10.1080/08916152.2015.1024352

[4] BAHRAMI, M., J. R. CULHAM, M. M. YANANOVICH and G. E. SCHNEIDER. Review of Thermal Joint Resistance Models for Nonconforming Rough Surfaces. *ASME Applied Mechanics Reviews Journal* [online][cit. 2019-05-03]. 2006, **59**(1), 1-12. ISSN 00036900 Available: doi:10.1115/1.2110231

[5] COOPER, M.G., B.B. MIKIC and M.M. YOVANOVICH. Thermal contact conductance. *International Journal of Heat and Mass Transfer* [online] [cit. 2019-05-03]. 1969, **12**(3), 279–300. ISSN 00179310. Available: doi:10.1016/0017-9310(69)90011-8

[6] CULHAM, J.R., P. TEERTSTRA, I. SAVIJA and M.M. YOVANOVICH. Design, assembly and commissioning of a test apparatus for characterizing thermal interface materials. In: *ITherm 2002. Eighth Intersociety Conference on Thermal and Thermomechanical Phenomena in Electronic Systems (Cat. No.02CH37258)* [online][cit. 2019-05-12]. IEEE Computer Society, 2002, 128–135. ISBN 0780371526. ISSN 19363958. Available: doi:10.1109/ITHERM.2002.1012448

[7] ČSN EN 4288:1999. Geometrické požadavky na výrobky (GPS) - Struktura povrchu: Profilová metoda – Pravidla a postupy pro posuzování struktury povrchu. Praha: Úřad pro technickou normalizaci, metrologii a státní zkušebnictví, 1999. 16 pages. Třídící znak 014449.

[8] ČSN EN 13601:2013. Měď a slitiny mědi-Tyče a dráty z mědi pro všeobecné použití v elektrotechnice. Praha: Úřad pro technickou normalizaci, metrologii a státní zkušebnictví, 2013. 28 pages. Třídící znak 42 1502.

[9] *ESA: New member states* [online] [cit. 2019-04-29]. Available: `http://www.esa.int/About_Us/Welcome_to_ESA/New_Member_States`

[10] *ESA: Our Missions* [online] [cit. 2019-04-29]. Available: `http://www.esa.int/ESA/Our_Missions`

[11] *ESA: What is ESA?* [online] [cit. 2019-04-22]. Last update: 20 March 2019. Available: http://www.esa.int/About_Us/Welcome_to_ESA/What_is_ESA

[12] ESA SOW HEAT SWITCH. *Statement of Work, Miniaturised Heat Switch, Annex 1: Preliminary Functional Specification*. European Space Agency: AG Noordwijk zh, The Netherlands, published: 11. 05. 2011, 24 pages. TEC-MTT/2011/3756/In/SL. Appendix 1 to ITT 1-6801/11/NL/NA

[13] ETTL, Peter, Berthold E. SCHMIDT, M. SCHENK, Ildiko LASZLO and Gerd HAEUSLER. Roughness parameters and surface deformation measured by coherence radar. In: RASTOGI Pramod K. and Ferenc GYIMESI (ed.). *International Conference on Applied Optical Metrology* [online][cit. 2019-05-12]. 1998, 1-8. DOI: 10.1117/12.323304. Available: https://www.researchgate.net/publication/260864215_Roughness_parameters_and_surface_deformation_measured_by_coherence_radar

[14] GADELMAWLA, E.S., M.M. KOURA, T.M.A. MAKSOUD, I.M. ELEWA and H.H. SOLIMAN. Roughness parameters. *Journal of Materials Processing Tech* [online]. Elsevier B.V, 2002, **123**(1), 133-145 [cit. 2019-05-12]. DOI: 10.1016/S0924-0136(02)00060-2. ISSN 0924-0136. Available: https://www-sciencedirect-com.ezproxy.lib.vutbr.cz/science/article/pii/S0924013602000602

[15] HEGAZY, Adel Abdel-Halim. Thermal Joint Conductance of Conforming Rough Surfaces: Effect of Surface Micro-Hardness Variation. *UWSpace* [online][cit. 2019-05-03]. 2016[1985]. Available: http://hdl.handle.net/10012/10844

[16] LAMBERT, M. A. and L. S. FLETCHER. Review of Models for Thermal Contact Conductance of Metals. *Journal of Thermophysics and Heat Transfer* [online][cit. 2019-01-14]. 1997, **11**(2), 129-140. Available: https://dokumen.tips/documents/review-of-models-for-thermal-contact-conductance-of-metals.html

[17] MADHUSUDANA, C. V. Thermal contact conductance. New York: Springer-Verlag,©1996. ISBN 0-387-94534-2

[18] MAJUMDAR, A. and C. L. TIEN. Fractal Network Model for Contact Conductance. *Journal of Heat Transfer* [online][cit. 2019-05-19]. 1991, **113**(3), 516-525. ISSN 00221481. Available: doi:10.1115/1.2910594

[19] MAL'KOV, V. A.. Contact thermal resistance of machined metal surfaces in vacuo. *Journal of Engineering Physics* [online] [cit. 2019-05-03]. 1970, **18**(2), 187–194. ISSN 0022-0841. Available: doi:10.1007/BF00828010

[20] MAŠEK, J. *Funkční zkouška tepelného spínače pro prostředí planety Mars*. Brno: Vysoké učení technické v Brně, Fakulta strojního inženýrství, 2016. 129 s. Vedoucí diplomové práce Ing. Robert Popela, Ph.D..

[21] MAŠEK, J.. Thermo-vacuum test chamber development for airborne and space equipment testing in simulated extreme conditions. In *ICAS 2018 - PROCEEDINGS* [online][cit. 2019-05-19]. ICAS 2018, Belo Horizonte, Brazílie: The International Council of the Aeronautical Sciences, 2018. 1-9. ISBN: 978-3-932182-88-4. Available: http://www.icas.org/ICAS_ARCHIVE/ICAS2018/data/papers/ICAS2018_0548_paper.pdf

[22] MAŠEK, J., M. HORÁK and P.ZIKMUND. Miniaturized Thermal Switch Report on BB Testing. *Report no: LU33-2017-MHS.PR.* ©Letecký ústav, VUT Brně, Date of release: 9.1.2018, 56 pages

[23] MAŠEK, Jakub, Daniel KOUTNÝ and Robert POPELA. Thermal conductivity of Cu7.2Ni1.8Si1Cr copper alloy produced via SLM and ability of thin-wall structure fabrication. In: *13th Research and Education in Aircraft Design: Conference proceedings* [online][cit. 2019-05-19]. Brno: Fakulta strojního inženýrstvi VUT v Brně, 2019, 119–129. ISBN 978-80-214-5696-9. Available: doi:10.13164/conf.read.2018.12

[24] MIKIC, B.B.. Thermal contact conductance; theoretical considerations. International Journal of Heat and Mass Transfer [online] [cit. 2019-05-03]. 1974, **17**(2), 205–214. ISSN 00179310. Available: doi:10.1016/0017-9310(74)90082-9

[25] MIKIC, B. B., and W. M. ROHSENOW. Thermal Contact Resistance. *NASA Contract NGR 22-009-065* [online] [cit. 2019-05-03]. 1966, 1-130. Available: `https://core.ac.uk/download/pdf/4425917.pdf`

[26] PAVELEK, Milan. Termomechanika. Brno: Akademické nakladatelství CERM. 2011, 1-192. ISBN: 978-80-214-4300-6.

[27] SAVIJA, I., J. R. CULHAM, M. M. YOVANOVICH and E. E. MAROTTA. Review of Thermal Conductance Models for Joints Incorporating Enhancement Materials. *AIAA Journal of Thermophysics and Heat Transfer* [online] [cit. 2019-05-03]. 2003, **17**(1), 43–52. Available: `http://www.mhtlab.uwaterloo.ca/pdf_papers/mhtl03-3.pdf`

[28] SHLYKOV, Yu.P. and Ye.A. GANIN. Thermal resistance of metallic contacts. *International Journal of Heat and Mass Transfer* [online] [cit. 2019-05-03]. 1964, **7**(8), 921–929. ISSN 00179310. Available: doi:10.1016/0017-9310(64)90147-4

[29] SONG, S. and M. YOVANOVICH. Relative contact pressure - Dependence on surface roughness and Vickers microhardness. *Journal of Thermophysics and Heat Transfer* [online][cit. 2019-05-03]. 1988, **2**(1), 43–47. ISSN 0887-8722. Available: doi:10.2514/3.60

[30] SRIDHAR, M.R. and M.M. YOVANOVICH. Elastoplastic Contact Conductance Model for Isotropic, Conforming Rough Surfaces and Comparison with Experiments *Journal of Heat Transfer* [online] [cit. 2019-04-29]. 1996, **118**(1), 1-14. Available: `http://www.mhtlab.uwaterloo.ca/pdf_papers/mhtl96-3.pdf`

[31] SRIDHAR, M.R. and M.M. YOVANOVICH. Empirical methods to predict Vickers microhardness. *Wear* [online] [cit. 2019-05-03]. Elsevier B.V, 1996, **193**(1), 91–98. ISSN 00431648. Available: doi:10.1016/0043-1648(95)06681-0

[32] SRIDHAR, M. R. and M. YOVANOVICH. Review of elastic and plastic contact conductance models: Comparison with experiment. *Journal of Thermophysics and Heat Transfer* [online] [cit. 2019-04-13]. 1994, **8**(4), 633–640. Available: `http://www.mhtlab.uwaterloo.ca/pdf_papers/mhtl94-3.pdf`

[33] SUNIL KUMAR, S. and K. RAMAMURTHI. Influence of Flatness and Waviness of Rough Surfaces on Surface Contact Conductance. *Journal of Heat Transfer* [online][cit. 2019-05-03]. 2003, **125**(3), 394-402. ISSN 00221481. Available: doi:10.1115/1.1565093

[34] THOMAS, T. R. and R. S. SAYLES. Random-process analysis of the effect of waviness on thermal contact resistance. Thermophysics and Heat Transfer Conference [online] [cit. 2019-04-29]. 1974, 1-8 Available: doi:10.2514/6.1974-691

[35] TIEN, C. L.. A Correlation for Thermal Contact Conductance of Nominally Flat Surfaces in Vacuum. In: *Proceedings of the 7th Conference on Thermal Conductivity, National Bureau of Standards, Special Publication 302* [online] [cit. 2019-05-03]. 1968, 755–759. Available: `https://www.govinfo.gov/content/pkg/GOVPUB-C13-801075c3533d8dcbbcf43c84cc8c4eca/pdf/GOVPUB-C13-801075c3533d8dcbbcf43c84cc8c4eca.pdf`

[36] WANG, Anliang and Jianfeng ZHAO. Review of prediction for thermal contact resistance. Science China Technological Sciences [online][cit. 2019-05-03]. 2010, **53**(7), 1798–1808. ISSN 1674-7321. Available: doi:10.1007/s11431-009-3190-6

[37] YOVANOVICH, M.M.. Four decades of research on thermal contact, gap, and joint resistance in microelectronics. *IEEE Transactions on Components and Packaging Technologies* [online][cit. 2019-04-13]. 2005, **28**(2), 182–206. ISSN 1521-3331. Available: doi:10.1109/TCAPT.2005.848483

[38] YOVANOVICH, M.M.. New contact and gap conductance correlations for conforming rough surafce. In: *AIAA Paper No. 81-1164, AIAA 16th Thermophysics Conference, Palo Alto, CA, June 23-25* [online] [cit. 2019-05-03]. 1981, 1-6. Available: `http://www.mhtlab.uwaterloo.ca/pdf_papers/mhtl81-1.pdf`

[39] YOVANOVICH, M. M.. Thermal Contact Correlations. *Progress in Astronautics and Aeronautics: Spacecraft Radiative Transfer and Temperature Control* [online] [cit. 2019-05-03]. 1982, **83**, 83–95. Available: `http://www.mhtlab.uwaterloo.ca/pdf_papers/mhtl82-1.pdf`

[40] YOVANOVICH, M.M., J.R. CULHAM and P. TEERTSTRA. Calculating interface resistance. *Electronics Cooling* [online][cit. 2019-05-03]. 1997, **3**(2), 24-29. Available: `http://www.mhtlab.uwaterloo.ca/pdf_papers/mhtl97-4.pdf`

[41] YOVANOVICH, M. M. and E. E. MAROTTA. Thermal Spreading and Contact Resistances. In: Bejan, A. and Kraus, A.D., (ed.). *Heat Transfer Handbook* [online] [cit. 2019-01-12]. 2003, 261-394. Available: `https://s3-ap-southeast-1.amazonaws.com/erbuc/files/5495_7423fcc8-2d44-4d68-8a51-a92003ec647c.pdf`

11 List of short cuts and symbols

BB	Bread Board
BUT	Brno University of Technology
CI	Cold Interface
CLA	Center Line Average
CMY	Cooper-Mikic-Yovanovich
CO_2	Carbon Dioxide
ESA	European Space Agency
HI	Hot Interface
MHS	Miniaturized Heat Switch
PCM	Phase Change Material
Ra	Arithmetic average height (surface roughness)
Rq	Root mean square surface roughness
RMS	Root Mean Square
TCC	Thermal Contact Conductance
TCR	Thermal Contact Resistance

12 List of Figures

13 List of Tables

14 Appendix

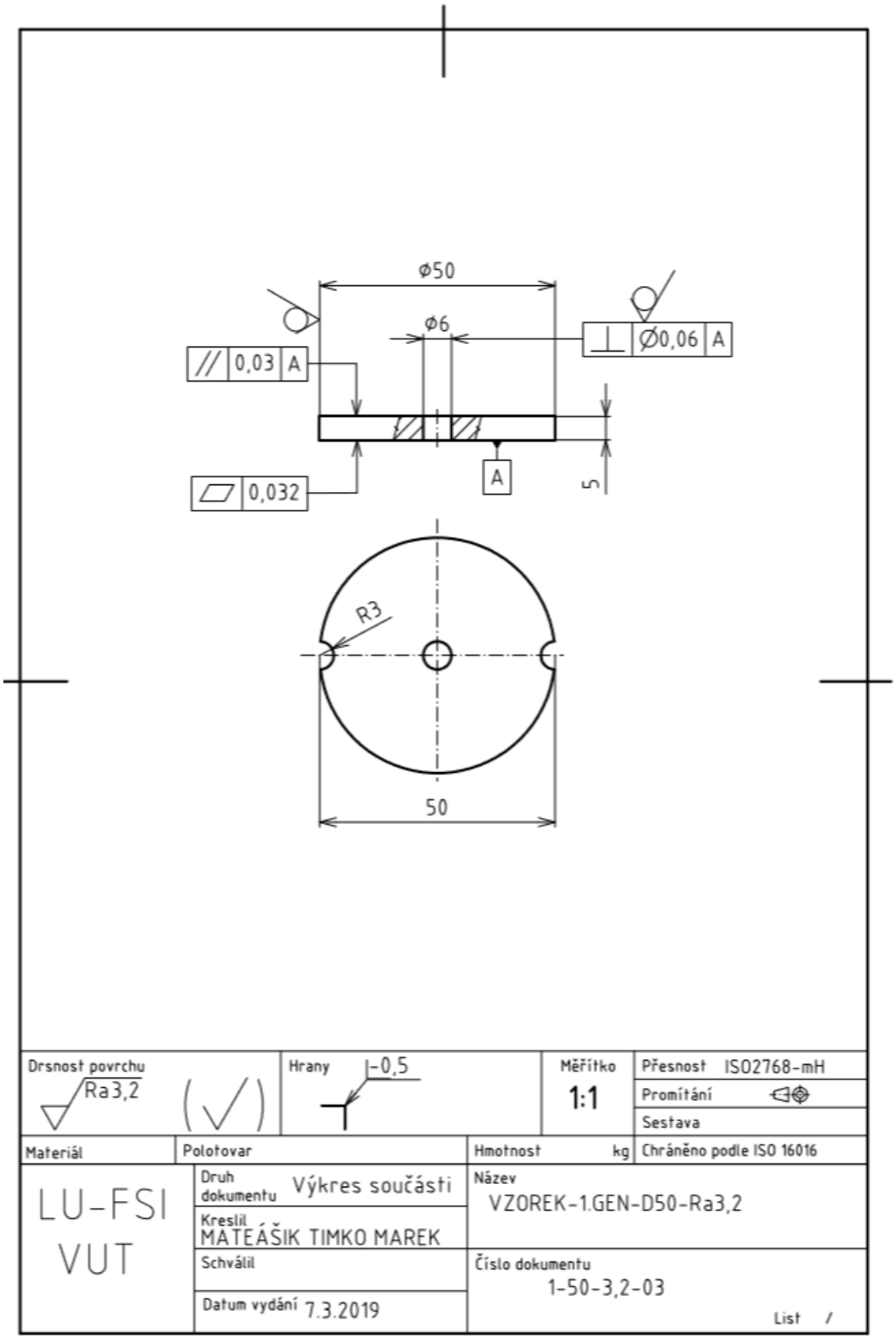

Figure 18: Mechanical drawing of specimen with diameter of 50 mm.

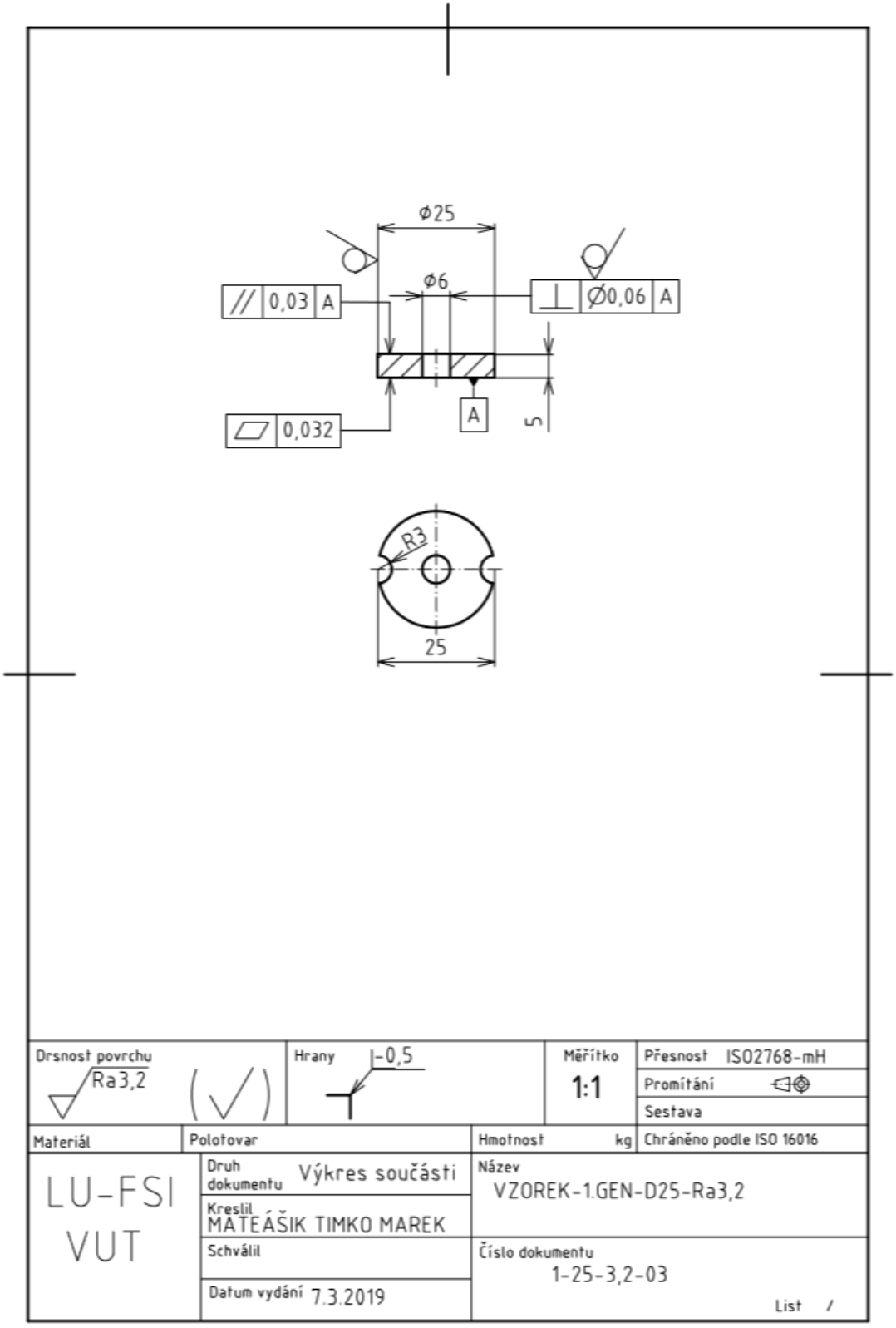

Figure 19: Mechanical drawing of specimen with diameter of 25 mm.

Figure 20: Specimen with diameter of 50 mm*, top view.*

Figure 21: Specimen with diameter of 50 mm*, side view.*

Figure 22: Specimen with diameter of 25 mm*, top view.*

Figure 23: Larger and smaller specimen in comparison, top view.

Figure 24: 3D printed holder for specimens.

Figure 25: Specimen gripped in holder.

Figure 26: Specimen surface measurement.

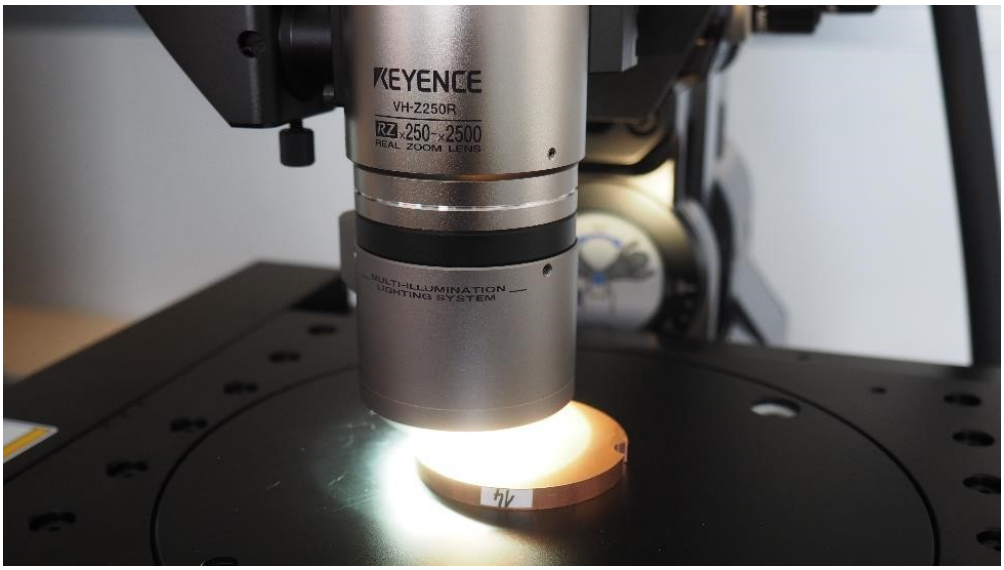

Figure 27: Specimen surface measurement, closer look.

Figure 28: Grinder polisher machine.

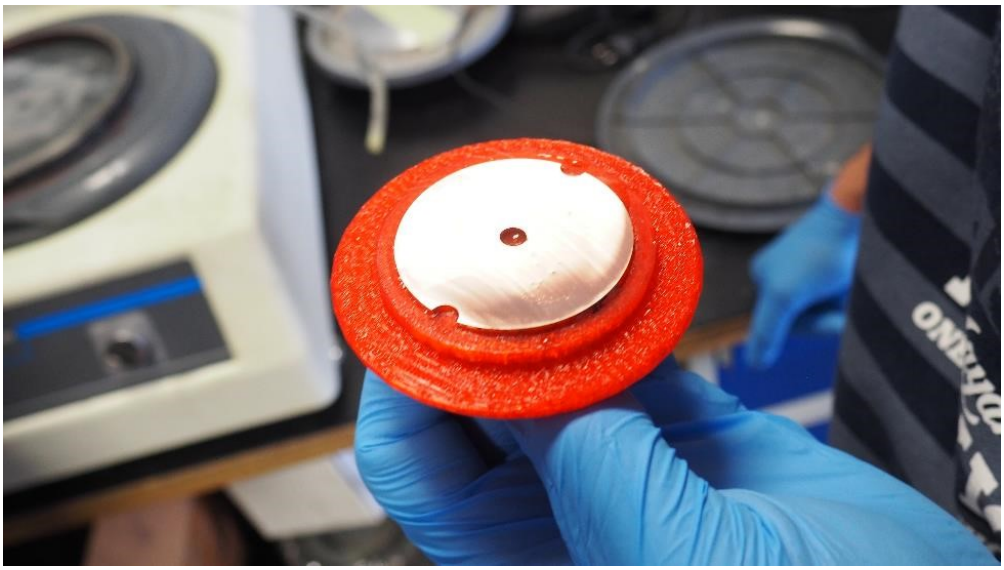

Figure 29: Grinded specimen.

*Figure 30: Grinded specimen with diameter of 50*mm*, top view.*

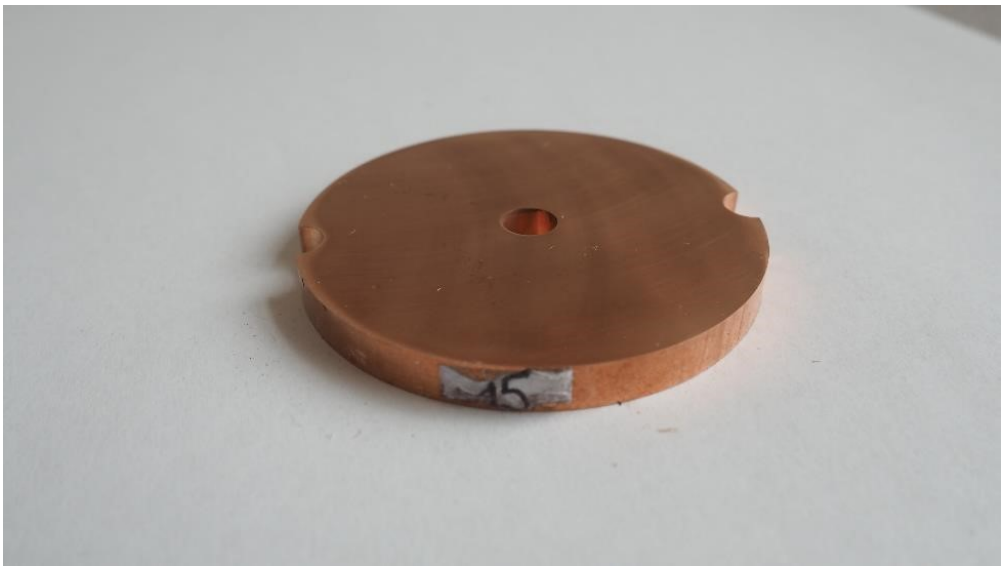

*Figure 31: Grinded specimen with diameter of 50*mm*, side view.*

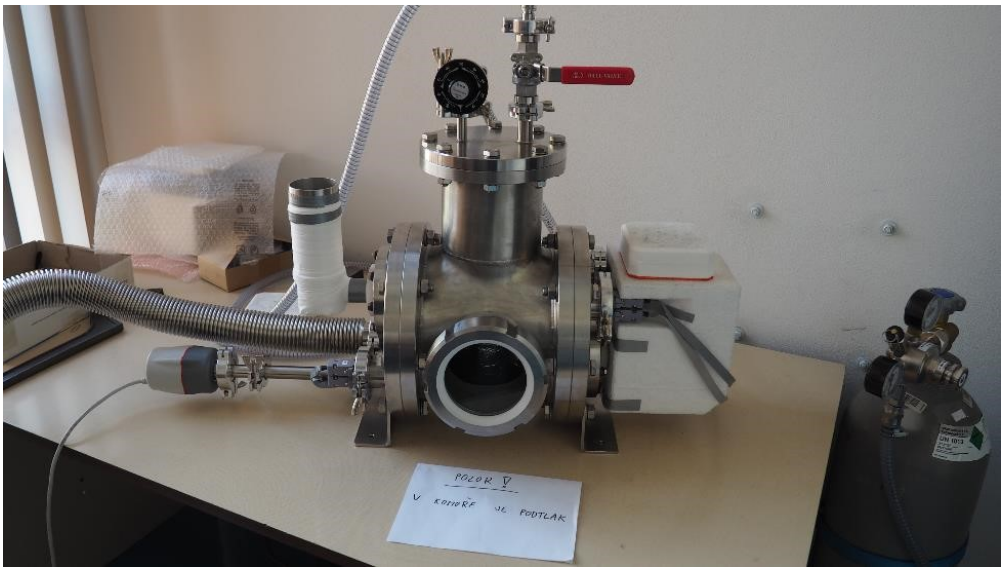

Figure 32: Test chamber

Figure 33: Specimens with shielding in test chamber.

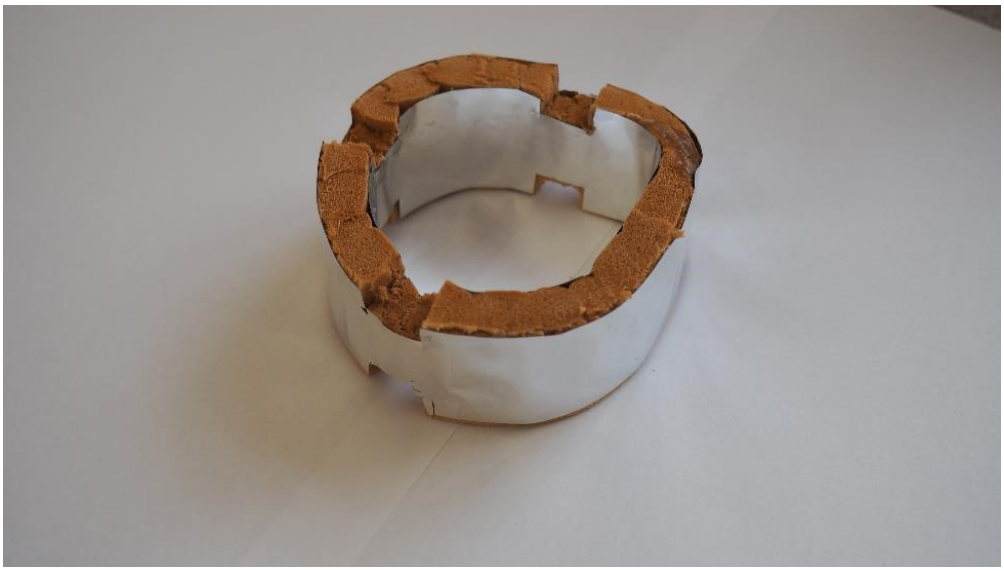

Figure 34: Upilex shielding.

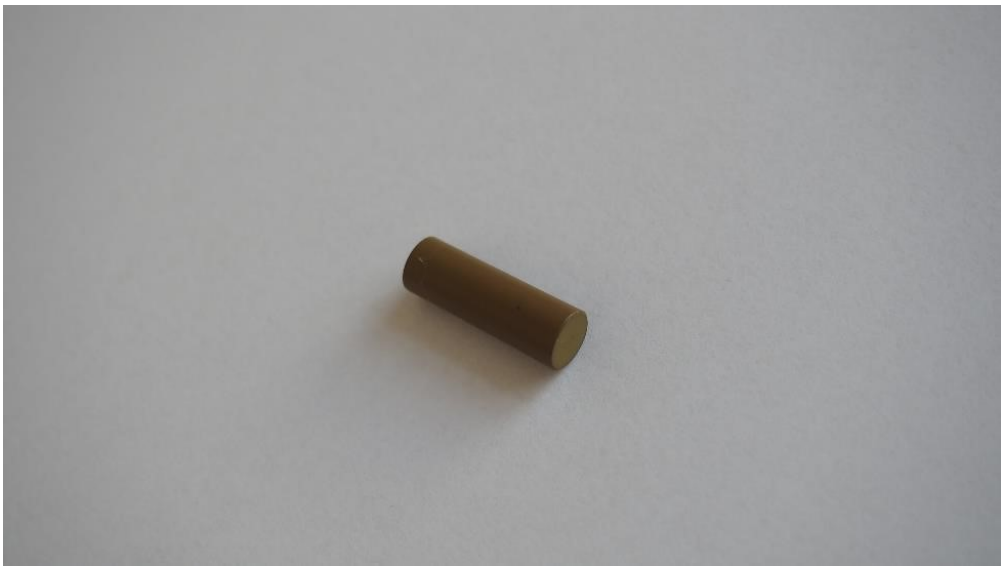

Figure 35: Torlon dowel.

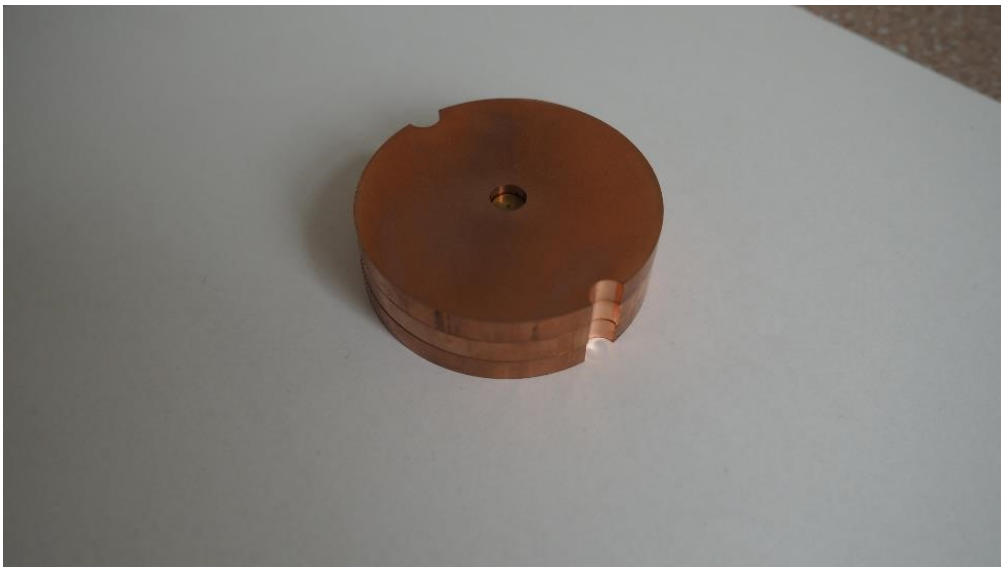

Figure 36: Stack with three specimens with diameter of 50 mm.

Figure 37: Stack with three specimens with diameter of 50 mm*, side view.*